Chapter 26
Hybridized Nanomaterials for Enhancing Photocatalytic Activity in Solar Fuel Production

Özlem Kap, Nesrin Horzum, and Canan Varlikli

Abstract Meeting the increasing demand for energy and clean water, access to these resources has become an essential requirement of modern human life. Nanohybrid material engineering is significant for the development of functional materials which can be used as photocatalyst. By optimizing the size, shape, and surface properties of such nanostructures, the photocatalytic process in terms of ensuring sustainable resource supply can be improved. The hybrid nanomaterials aim to obtain a high visible light absorption and low charge recombination resulting in a superior efficiency of photocatalytic reactions. The application areas which benefit from such nanohybrid materials are the filtration and degradation of organic pollutants and the photochemical hydrogen production for solar water splitting. This chapter describes in detail the nanohybrid materials including metal oxides, carbon-based materials, metal sulfides, metal–organic frameworks, and transition metal phosphides as well as bandgap tuning based on these structures, which affect the efficiency of photocatalysis.

Keywords Photocatalytic activity · Energy conversion · Photocatalytic degradation · Nanohybrid materials · Heterostructure · Solar fuel

Ö. Kap (✉) · N. Horzum
Engineering Sciences Department, İzmir Katip Çelebi University, İzmir 35620, Turkey
e-mail: ozlem.kap@ikc.edu.tr

N. Horzum
e-mail: nesrin.horzum.polat@ikc.edu.tr

Ö. Kap
Physics of Complex Fluids, Faculty of Science and Technology, MESA+ Institute for Nanotechnology, University of Twente, Enschede 7500AE, The Netherlands

C. Varlikli
Department of Photonics, İzmir Institute of Technology, Urla, İzmir 35430, Turkey
e-mail: cananvarlikli@iyte.edu.tr

S. Garg and A. Chandra (eds.), *Green Photocatalytic Semiconductors*,
Green Chemistry and Sustainable Technology,
https://doi.org/10.1007/978-3-030-77371-7_26

26.1 Introduction

The non-renewable energy resources reserve mainly constituted of fossil fuels have a limited source and might be run out in the near future, causing an energy crisis [121]. Besides, the pollutant gases have produced by these fossil resources threaten global life due to contamination of air and climate change [38, 159]. Therefore, it has become important to improve the use of renewable resources which can supply the energy demand of the world. While the sources such as wind, biomass, hydro, geothermal, which have all renewable energy potential, have a strong production performance, the solar energy potential is relatively high, and it differs from the others remarkably given the capacity [193].

In recent years, the production of fuels such as hydrogen, methanol, and methane produced by converting solar energy into chemical energy has become a very rational approach to meet the energy demand and to cope with the environmental challenges. Photoelectrochemical (PEC) water splitting and CO_2 reduction is performed by using different semiconductor nanostructures as a photocatalyst to perform the solar-to-fuel conversion. Figure 26.1a shows the primary mechanism of water splitting by using a semiconductor photocatalyst. This mechanism works as follows: when a photocatalyst exposed the light which is greater or equal to its bandgap energy, absorbs the photons. Thus electrons and holes are formed bounded by Coulomb forces on the valance band and conduction band, respectively [233]. The semiconductor utilizes a proton to excite an electron from valance band to the conduction band in an excited state. The exposed light excites the electrons into the conduction band by leaving behind the holes in the valance band, as seen in Fig. 26.1b. An oxidation–reduction reaction proceeds during the exposure of the light. The charge carriers dissociate in a catalyst-liquid interface to produce hydrogen and oxygen from water molecules. However, one of the challenges during

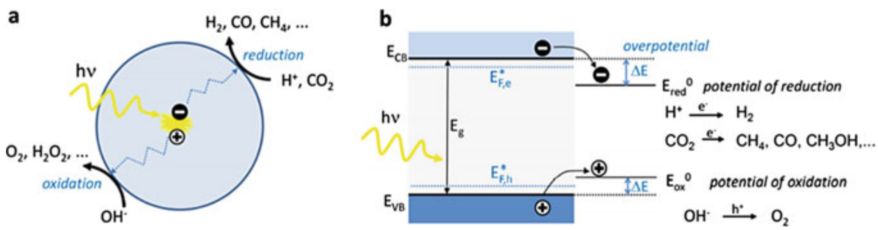

Fig. 26.1 **a** Photocatalytic processes on semiconductor nanomaterial involving photoexcitation and formation of electron−hole pair in the nanomaterial. The charges separately diffuse to the surface, where they can participate in reduction and oxidation reactions, respectively; **b** Energy diagram of the same process for a semiconductor with conduction band minimum located at E_{CB} and valence band maximum at E_{VB}, separated by a bandgap E_g. The overpotentials, ΔE, shown in blue, provide the driving force for the transfer of the charges to the electron acceptor (reduction) and donor (oxidation) molecules. the Fermi levels of the electrons and the holes are elevated to so-called quasi-Fermi levels, corresponding to Fermi levels under illumination (from Ref. [233] with permission from American Chemical Society)

the reaction is that the electrons and holes recombine on the catalyst surface, which resulted in low conversion efficiency.

In order to increase the photoconversion efficiency of the semiconductor nanomaterials, some methods used have led to the emergence of different strategies. These strategies may involve changing the shape, size, composition, and thus the active surface sites of the semiconductor photocatalysis [15]. It may involve doping method, surface functionalization, or forming a new interface with different nanomaterials as a heterostructure [190]. Therefore, the electronic band structure of the material would differ, and the solar-to-fuel efficiency would result in various efficiency depending on the bandgap engineering of the material. The required minimum energy transfer to achieve water splitting should be 1.23 eV per electron, according to Nernst's equation [254]. Thus, the photocatalyst to be used must absorb solar light photon energy greater than 1.23 eV. In a photoanode to conduct the oxygen evolution reaction (OER), the valence band must be more positive than the O_2/H_2O potential. In contrast, in a photocathode, the hydrogen evolution reaction (HER) would be conducted with more negative potential than the H^+/H_2 potential [227]. The band edge positions of different materials are shown in Fig. 26.2.

The requirement to perform an effective PEC water splitting and to commercialize it is to increase light-to-energy conversion efficiency. Until today, studies have been carried out on the development of low-priced, non-toxic, stable, and efficient semiconductor materials that can absorb the light in the visible region of the electromagnetic spectrum. It should be noted that the solar light, which is a green energy source by itself, is also included in the scope of green energy in the many synthesis methods of photocatalysts used to harvest it.

Many literature studies, in which all configurable and hybrid combinations of nanomaterials have been investigated using as a photocathode or photoanode in overall solar water splitting reaction to increase efficiency as a photocatalyst. This book chapter focuses on recent studies on solar-to-fuel conversion because of the

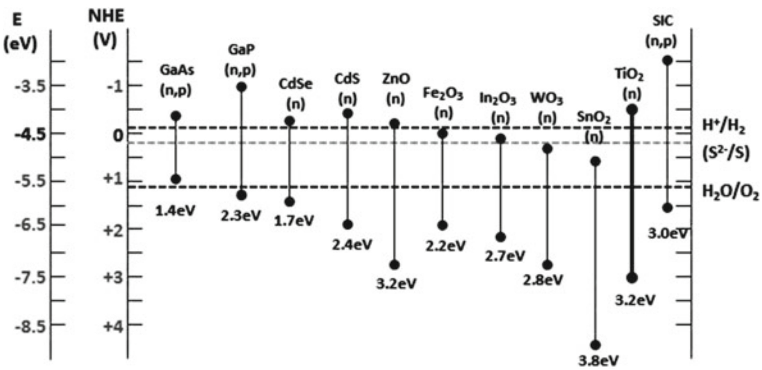

Fig. 26.2 Band edge positions of semiconductors and their relevance with photocatalytic H_2 generation

highly efficient nanomaterials such as metal oxides, metal–organic frameworks, carbon-based materials, metal sulphides, and phosphides which have been used mostly for photoelectrochemical water splitting applications. The factors which reduce the efficiency of solar conversion will be discussed based on the electron–hole recombination, limited photon absorption, and charge separation efficiency for the mentioned nanomaterials. This chapter has been evaluated for water splitting and CO_2 reduction application of the nanomaterials, however, it should be noted that the same structures can also be used for photocatalytic degradation application.

26.2 Metal Oxides

In this section, we aim to focus on the use of hybridized metal oxide nanomaterials in the study of photocatalysis for hydrogen generation from water splitting, pollutant degradation, and greenhouse gas reduction. Nanostructured metal oxides are ideal photocatalysts due to their high surface area, reactive sites, bandgap, and morphology [116, 213]. The metal oxide first remembered as a photocatalyst is titanium dioxide (TiO_2) with its non-toxicity, chemical stability, and high photocatalytic activity. However, one disadvantage is the wide bandgap (3.2 eV) that makes TiO_2 only sensitive to the ultraviolet (UV) region [48]. Another disadvantage is the fast electron–hole recombination and its relatively poor charge-carrying ability, resulting in low quantum efficiencies [96, 169]. Several approaches have been used to modify TiO_2 materials to overcome these disadvantages. Not only morphological modifications such as the production of TiO_2 nanomaterials with larger surface area, but also chemical modifications which include metal, non-metal, metal- non-metal, metal oxide doping, immobilization of TiO_2 on secondary substrates, and the use of nanomaterials as TiO_2 support, composite fabrication with semi-conductors have been applied to increase photocatalytic activity. In this context, some studies which have been conducted in recent years are classified in Table 26.1.

Doping is one of the frequently used methods to increase the photocatalytic activity of TiO_2 by reducing the bandgap and constructing new energy levels. The proper amount of doping will reduce the recombination of photogenerated charges, but when used excessively, they act as a recombination center [5]. One of the favorite metal doping for TiO_2 semiconductor is iron which is non-toxic, inexpensive, and earth-abundant element. Because the ionic radius of iron is very close to the TiO_2 lattice parameter [306], in this case, it can also be doped easily. However, the iron doping process requires precise control during synthesis. Xu et al. showed that the photocatalytic performance of Fe-doped TiO_2 varies depending on the method of synthesis, iron precursor, and iron concentration which cause the changes in porosity, particle size, and morphology [291]. The CH_4 formation yield was 0.23 μmol g^{-1} h^{-1} under visible light illumination for Fe-doped TiO_2. Its specific surface area and bandgap were 275 m^2 g^{-1}, 2.75 eV, respectively. Fe-TiO_2-500 was synthesized via one-step hydrothermal method at 500 °C. BET

Table 26.1 The chemical modification classification for TiO_2

Chemical modifications			
Metal doping	Bimetal doping	Metal oxide doping	Metal/non-metal doping
Silver (Ag) [69], Aluminium (Al) [191] Cobalt (Co) [307] Chromium (Cr) [170] Copper (Cu) [41] Erbium (Er) [226] Gallium (Ga) [152] Lanthanum (La) [145] Magnesium (Mg) [179] Molybdenum (Mo) [115] Manganese (Mn) [236] Nickel (Ni) [110] Niobium (Nb) [173] Palladium (Pd) [212] Platinum (Pt) [39] Rhodium (Rh) [108] Ruthenium (Ru) [4] Antimony (Sb) [133] Tin (Sn) [228] Strontium (Sr) [326] Terbium (Tb) [274] Vanadium (V) [194] Tungsten (W) [137] Ytterbium (Y) [14] Zinc (Zn) [104] Zirconium (Zr) [46]	Au–Ag [304] Bi–Y [76] Cu–Ni [160] Cu–Zn [160] Fe–Ni [240] Ni–Bi [183] Ni–Cr [218] Ni–Si [129] Mn–Zn [276] Er–W [113] La–Nb [75] Rh–Sb [106] Sn–La [343] Sr–Rh [184] Zr–Ag [180] Zr–Pd [46]	Cu_2O [296] Fe_2O_3 [177] MoO_3 [109] NiO [112] PdO [105] PtO [174] SnO_2 [83] WO_3 [66] V_2O_5 [198] ZnO [189] ZrO_2 [157]	Fe–N [54] Ag–N [316] K–Na–Cl [45]
	Nanomaterials supported on TiO_2	**Hybrid TiO_2 nanostructures**	**Non-metal doping**
	Ag nanoparticles [332] Au nanoparticles [187] Au–Pd nanoparticles [42] Bi nanoparticles [333] Cu nanoparticles [210] CuO nanoparticles [312] Pd–Au nanoparticles [224] PdCoNi nanoparticles [24] Pt nanoparticles [234] Pt–Pb nanoparticles [9] SnO_2 nanostructures [256]	Graphitic carbon nitride (g-C_3N_4)–Pt–TiO_2 [313] TiO_2 supported MOF-199 derived Cu–Cu_2O nanoparticles [158] g-C_3N_4 nanosheet hybridized N-doped TiO_2 nanofibers [77] TiO_2/FeMnP core/shell nanorod [216] Pd-decorated hierarchical TiO_2 constructed from the MOFs NH_2-MIL-125(Ti) [300] Cu/TiO_2/$Ti_3C_2T_x$ [192] NH_2-MIL-125(Ti)/TiO_2 [309] Cu/TiO_2 core−shell heterostructures derived from Cu-MOF [176] TiO_2 nanorod mats surface sensitized by cobalt ZIF-67 [56] Fe_2TiO_5–TiO_2 [321] MOF-derived TiO_2 photoanodes sensitized with quantum dots (CdSe@CdS) [221] Ru species supported on MOF-derived N-doped TiO_2/C hybrids [299]	Carbon (C) [130] Nitrogen (N) [107] Phosphorus (P) [171] Sulfur (S) [197] Selenium (Se) [287] Fluorine (F) [17] Chlorine (Cl) [270] Bromine (Br) [265] Iodine (I) [215] N–S [58] C–N–S [51]
			TiO_2 supported on secondary substances
			Activated carbon fibers (ACFs) [64] Carbon nanotubes (CNTs) [10] Graphitic carbon nitride (g-C_3N_4) [229] Graphene [79] Graphene oxide [249] Silica [196] Aluminium silicate [95] Zeolite [315] Biochar [317] Poly(methyl methacrylate) nanofibers [134] Poly (styrene-co-vinylphosphonic acid) fibers [88]

specific surface area was 202 m^2, and the bandgap was of 2.42 eV. The bandgap and porosity reduced by the chancing the synthesis condition, which results in an increase of the CH_4 formation rate as 0.47 μmol g^{-1} h^{-1}.

The concentration of metal doping affects the photocatalytic activity of doped-TiO_2 since the metal doping may tune the anatase–rutile transformation during the synthesis [5]. Anatase is the indirect bandgap semiconductor, whereas rutile is direct bandgap semiconductor. Indirect bandgap anatase exhibits a longer lifetime of photoexcited electrons and holes. It has been shown that anatase has the lightest effective mass, which helps the fastest migration of photogenerated electrons and holes from the inside to surface of anatase TiO_2 by lowering the recombination rate of photogenerated charge carriers. Therefore, anatase TiO_2 has a higher photocatalytic activity than rutile TiO_2 [319].

Rutile and anatase have a band of 3.0 and 3.2 eV, respectively. Ding et al. have formed a heterojunction with these two phases, and the internal electric field has been built with two different work functions of anatase and rutile. They showed that the heterophase junction constructed by using TiO_2 nanobelt increases photocatalytic activity [49]. Figure 26.3 is a schematic illustration of the photocatalytic mechanism owing to the heterophase junction. Moreover, the O_2 production rate was investigated with increasing calcination temperature. The highest O_2 evolution rate of 0.352 mmol h^{-1} g^{-1} was obtained due to the formation of anatase/rutile heterophase junctions connections at 900 °C. TiO_2 nanobelt calcinated at 600, 700, 800 °C were pure anatase, at 1000 °C was of pure rutile, and the O_2 evolution rate is 0.09, 0.124, 0.16 and 0.198 mmol h^{-1} g^{-1}, respectively. Thus, constructed anatase/rutile heterophase junctions enhanced carrier separation efficiency and carrier recombination suppress.

Some non-metallic element dopings which are most commonly used in the literature have been listed in Table 26.1. Non-metallic doping increases the light absorption in the visible region of TiO_2, enhancing the electron–hole separation, but again they act as recombination centers due to the formed oxygen vacancies [5]. However, it was stated that the performance of the non-metallic doping could not enhance the photocatalytic activity as much as metallic doping [96]. The advantage

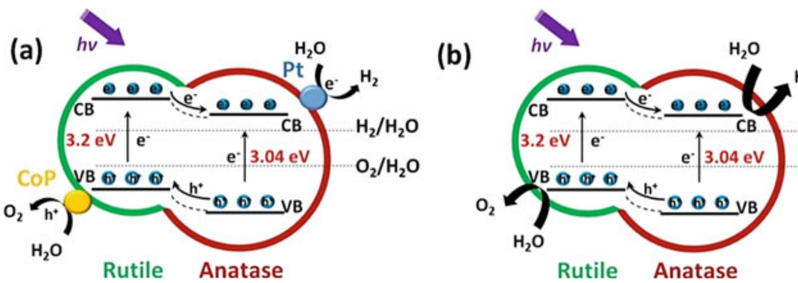

Fig. 26.3 Schematic illustration of the photocatalytic mechanism of the rutile/anatase heterophase junction **a** with and without Pt/CoP cocatalysts (Reprinted from Ref. [49] with permission from Elsevier)

of the non-metallic doping to metals does not act as electron traps, and they have been used to improve photocatalytic activity by using this feature [298].

The p-states of the non-metallic elements mix with the O-2p states of TiO_2 which causes redshift on the valance band and the bandgap decreases. Nitrogen is one of the most frequently used as dopants for TiO_2. Likewise, C doped TiO_2 also enables the formation of new energy levels above the valence band, so the lower absorption spectrum shifts to the higher wavelengths [12]. F-doped TiO_2 is another non-metal doping element, and they occupy the oxygen vacancies which are in the lattice rather than doping into the TiO_2. Thus, electron–hole recombination sites are reduced by fluorine. Moreover, Du et al. stated that the reason why F doping decreases photocatalytic activity is that element F causes surface fluorination, not doping [55]. A very high photocatalytic activity has been obtained by the F doping method by using Mesoporous mesocellular foams as support for fluorine atoms in a study. In order to increase the substitution of these atoms, the vacuum activation method was used to boost the oxygen vacancies in TiO_2, thus yielding Ti^{3+}-F lattice structures.

The F-doped catalyst exhibits high photocatalytic activity and stability for H_2 evolution under solar light irradiation with an AM 1.5 air mass filter. The success of the technique attributed to the decrease of recombination sites by high concentration F doping and the synergistic effect between lattice Ti^{3+}-F and surface Ti^{3+}-F [289]. Other single metal oxides used for photocatalytic applications other than TiO_2 include ZnO [57, 87, 93], CeO_2 [85], CuO [203], Cu_2O [283], SnO_2 [186, 225], Fe_2O_3 [82], NiO [139], MoO_3 [205, 344], WO_3 [217], ZrO_2 [68], Ag_2O [268], Bi_2O_3 [266], In_2O_3 [90]. Besides defect engineering strategies such as surface hydrogenation, metal reduction, and thermal treatment to create oxygen vacancies, heterostructure engineering is considered to be another effective way of obtaining photocatalysts with improved efficiencies [11]. For example, metal catalysts (Au, Pt, Pd, Cu) and bimetallic catalysts (Au–M (M=La, Ni, Cu, Fe, Cr, Y), Pt–Cu, Pd–Cu) are supported on various single and dual metal oxides to enhance the light absorption capacity under UV light due to the Schottky barrier and SPR [40]. The photocatalytic activity of the metal oxides can be improved by not only changing the morphology (i.e., obtaining nanostructures with a core/shell structure) but also using binary metal oxides (ZnO/V_2O_5 [8], ZnO/In_2O_3 [43], CeO_2 supported on SiO_2 fibers [89], Fe_2O_3/TiO_2 [16], Fe_2O_3/WO_3 [178], ZnO Nanorod/α-Fe_2O_3 [251], NiO/V_2O_5 [175], Bi_2O_3–$BiFeO_3$ [163], SnO_2/ZnO [341], WO_3–$BiVO_4$ nanostructures [120]) with higher oxygen mobility over the surface, visible light activity. Besides precious metals decorated binary metal oxides, ternary metal oxide nano-photocatalysts (CuO/CeO_2/ZnO [151] $Bi_2O_3/Bi_2SiO_5/SiO_2$ microspheres [320]) with more efficient photocatalytic performance have been studied. Moreover, QDs, carbon nanotubes, g-C_3N_4 are used as sensitizers for photocatalytic metal oxide structures such as ZnO/CdS [3], ZnO/CdTe [156], MoO_3-MWCNT [219] ZrO_2/g-C_3N_4 [94], etc. An important class of metal oxide catalysts in green energy production is perovskite oxides (such as titanate-based perovskites; $ATiO_3$ (A=Ba, Ca, Co, Cu, Fe, Mg, Mn, Ni, Pb, Sr, Zn), tantalite-based; $KTaO_3$, $NaTaO_3$, and other-metal-based perovskite oxide photocatalysts like $BaZrO_3$, $LaFeO_3$, and $LaMnO_3$ because of their excellent absorption, bandgap tunability, and water splitting [185].

26.3 Carbon-Based Nanomaterials

26.3.1 *Graphene-Based Nanomaterials*

Graphene (G) consists of a single layer of sp^2 hybridized carbon atoms, arranged in a 2D honeycomb lattice. In addition to being the thinnest material known, it is also the most robust material with a 1GPa Young' modulus [117]. Graphene synthesis can be carried out either by the top-down approach via mechanical, chemical, or electrochemical exfoliation methods or by the bottom–up approach via chemical vapor deposition and chemical synthesis methods [20]. In Table 26.2, the methods used to synthesize graphene-based structures are summarized, additively, the synthesis methods of composite structures have also been shown.

Graphene has drawn attention in solar fuel applications due to excellent properties such as high stability, large specific surface area, the strong adsorption capacity, high thermal and electrical conductivity [6]. The high surface area contributes to the stabilization of the metal NPs, metal oxide, and quantum dot structures because the expanded π orbitals of G overlap with the d orbitals of the metallic structures [6]. Thus, it can be seen from the literature studies shown in Table 26.2; the formed heterojunction contributes to the photocatalytic conversion efficiently.

A well-known structure among various graphene derivatives is graphene oxide (GO) which is obtained by the oxidation of graphene. Contrary to the hydrophobic nature of graphene, GO containing hydrophilic functional groups (hydroxyl, carbonyl, carboxyl, epoxide) eliminates the problem of aggregation in aqueous solutions [47]. GO has low electrical conductivity; however, it is increased by the reduction of GO [21]. In a study, Zhu et al. used Ag NPs, CdS NRs, and reduced graphene oxide(rGO) composite material as photocatalyst for CO_2 reduction [345]. According to the result, it was determined that CO_2 adsorption capacity of CdS was 5.01 $cm^3\ g^{-1}$, while rGO–CdS and Ag–rGO–CdS were 6.60 and 6.02 $cm^3\ g^{-1}$, respectively. Increased adsorption indicates the positive contribution of RGO's high electrical conductivity, p–p conjugation between the rGO and CO_2, higher surface area (46.2 m^2g^{-1}) and large surface active sites. Moreover, both Ag and RGO act as the electron acceptor, which expedite in the CO_2 reduction reaction.

The degree of the reduction of GO can change the bandgap of the material, which is essential in the photocatalytic applications [2]. The optical band gap obtained by incorporation of G/GO into different materials is shown in Table 26.2. It has been reported in the studies the existence of G or GO resulted in narrowed the bandgap [74, 102, 141, 201, 220, 231, 242, 269, 335]. As a result of the bandgap calculation with the Tauc plot analysis, Sorcar et al. found that doped GO amount with 0.25, 0.50, or 0.75 ml to the reduced blue titania (RBT) reduced the bandgap to 2.61, 2.41, 2.22 eV, respectively, which was 2.68 eV for pure RBT [231]. While the produced C_2H_6 and CH_4 amount increased for 0.25 and 0.50 doping, and it decreased compared to the two for 0.75 doping. Similarly, Wang et al. detected CH_4

Table 26.2 Typical photocatalytic H_2-production systems of graphene-based nanomaterials

Catalyst	Synthesize-preparation method	Optical bandgap (eV)	Application	Products/Activity ($\mu mol \cdot g^{-1} \cdot h^{-1}$)	References
Graphene/TiO_2/Mo	Sol–gel for composite	2.62	Decomposition of methylene blue	–	[102]
Graphene/TiO_2	Drop-casting for graphene film on FTO-glass/magnetron sputtering, thermal treatment for composite	–	Photoelectrochemical (PEC) water splitting	–	[252]
$PbBiO_2Br$/GO	Hydrothermal synthesis for composite	2.40	Removal of CO_2, crystal violet dye and 2-hydroxybenzoic acid	CH_4/1.193	[141]
TiO_2/GO/rGO	Electrochemical anodization for TiO_2, UV-A radiation for reduction of GO, reflux process for GO and rGO functionalization	–	Photocatalytic reduction of CO_2	CO_2/760 μmol g^{-1}	[204]
Defective Graphene/NiO/Ni NPs	Pyrolysis for graphene, thermal treatment for composite	–	Photoassisted CO_2 reduction by H_2	CH_4/642.66	[165]
Graphene/UIO-66-NH_2	Hydrothermal synthesis and microwave-irradiation induced solvothermal synthesis for composite	2.64	CO_2 photo-reduction under visible-light	CO_2/42.6 μmol	[269]
rGO/CdS/ZnO	In-situ growth	2.12	Synthesis of the efficient hybrids for photocatalytic or PEC hydrogen generation	H_2/ 0.79 μmol cm^{-2} h^{-1}	[335]
N-doped defective graphene/RhCrOx /STO:Al	Pyrolysis for graphene, impregnation for composite	–	Produce a hybrid material for efficient photocatalyst	H_2/6375 O_2/3080	[167]

(continued)

Table 26.2 (continued)

Catalyst	Synthesize-preparation method	Optical bandgap (eV)	Application	Products/Activity (μmol·g^{-1}·h^{-1})	References
rGO/Rh_2O_3/Rh NPs	Hummers method for GO, Hydrothermal, thermal treatment for composite	–	CO_2 photoreduction	CH_4/814.38	[101]
Graphene/Cu_2O	Pyrolysis for graphene	–	CO_2 reduction	H_2/ 2031 μmol cm^{-2} h^{-1}	[91]
rGO/TiO_2	Reflux and vacuum thermal treatment for composite	2.36	Photocatalytic reduction of CO_2 into solar fuel	CH_4/12.75	[220]
N-doped rGO/ TiO_2/$ZnFe_2O_4$	Hummers method for graphene oxide, hydrothermal synthesis for composite	2.98	Degradation of reactive Yellow 86 and methanol oxidation	H_2/2481	[242]
Graphene/CeO_2/ CuO/QDs	Calcination for graphene	1.75 (CuO–G) 2.70 (CeO_2 –G)	Synthesis highly efficient material for solar-driven hydrogen production	–	[201]
rGO/$CoFe_2O_4$/ TiO_2	Hummers method for GO, Ultrasound-assisted wet impregnation for composite	3.20 (TiO_2–G) 1.38 ($CoFe_2O$–G)	Synthesis stable photocatalyst for high production of hydrogen	H_2/76559	[74]
N- and Co-doped graphene/TiO_2	Hydrothermal synthesis for TiO_2, sonochemical and calcination methods for composite	–	Photocatalytic generation of H_2O_2 within the visible light range	H_2/677.44	[307]
Graphene/Cu_2O	Pyrolysis for graphene	–	Photoassisted methanation	CH_4/14930	[164]
Graphene/ reduced blue titania/Pt NPs	Annealing the mixture of graphene and RBT, Pt photo deposited composite	2.22	Photoconversion of CO_2 to CH_4 and C_2H_6	CH_4/37 C_2H_6/11	[231]

(continued)

Table 26.2 (continued)

Catalyst	Synthesize-preparation method	Optical bandgap (eV)	Application	Products/Activity ($\mu mol \cdot g^{-1} \cdot h^{-1}$)	References
Graphene/ chlorophyll Cu	Film preparation method	2.66	Conversion of CO_2 to C_2H_6	C_2H_6/68.23	[282]
GO/Benzidine	Hummers' method for graphene, hydrothermal synthesis for composite	–		H_2/690	[339]
Multilayer Graphene/Gold nanoplatelets	Pyrolysis for composite	–	Synthesize an efficient photocatalyst for water splitting	H_2/1200000	[166]
Graphene nanoribbon/CdS	Solvothermal method for composite	2.17	H_2 evolution under visible-light illumination	H_2/1890	[285]

evolution for G-doped UIO-66-NH_2, and the evolution decreased for UIO-66-NH_2/3.0GR compared to UIO-66-NH_2/2.0GR [269]. The reason for the reduction is attributed to the excessive graphene which covers the active regions of the MOF structure. It is understood from the results that the optimum amount of G/GO doped materials increase the CH_4/H_2 evolution.

Any other G-doped nanostructure is bismuth oxyhalides, which are materials that may be the candidates for third-generation solar cell, can provide photocatalytic activity with visible light [305]. Recently, $PbBiO_2Br$/GO composite was produced via hydrothermal method as a new novel material with different grams of GO [141]. The morphology can be seen in Fig. 26.4. The bandgap energy of the composite was to 2.40 eV, which was lower compared to 2.47 eV bandgap energy of $PbBiO_2Br$. Thus, the composite material increased the photocatalytic conversion rate from CO_2 to CH_4. This change has been attributed to the double-bond resonant structure of GO which transports photo-generated electrons and suppresses the electron–hole recombination of the photocatalyst. Although the conversion of CO_2 to CH_4 is thermodynamically favorite, the requirement of 8 electrons makes this process kinetically complicated this process compared to the CO conversion, which requires 2 electrons transfer. In a study in which CO_2 conversion to CO was carried out by using multi-leg TiO_2 nanotubes wrapped with GO and rGO layer [204].

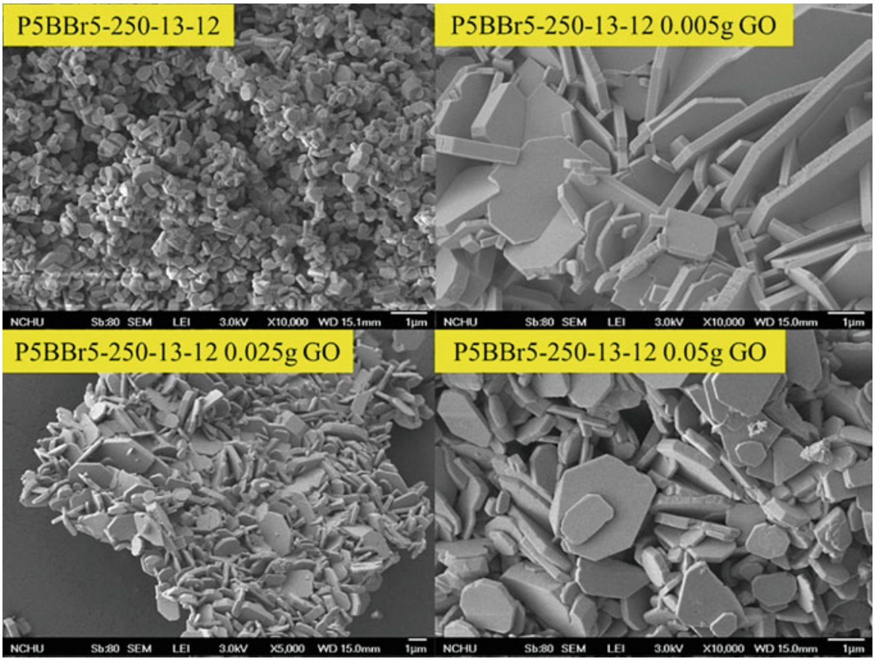

Fig. 26.4 SEM images of as-prepared samples by the hydrothermal autoclave method at different grams of GO (Molar ratio Pb:Br = 5:5, temp = 250 °C, time = 12 h) (Reprinted from Ref. [141] with permission from Elsevier)

Multi-leg TiO_2 nanotubes wrapped with GO and rGO were exposed to CO_2 for different periods. The rate of CO formation was observed to remain at the highest level (760 μmol g^{-1}) after 120 min for rGO wrapped nanotubes when compared to GO wrapped and bare multi-leg TiO_2 nanotubes. The high CO formation has been attributed to the electrical conductivity of GO/rGO layers connecting adjacent nanotubes which increased interaction between adsorbed CO_2 and photo-generated electrons.

The most important advantage of using graphene-based nanomaterials is that it increases the energy conversion by enhancing the photoabsorption and electron–hole separation with its high surface area. Moreover, the absorption spectrum of doped graphene and graphene with layer stacking defects extends from UV to NIR, which makes them an important class of material candidates for photocatalysis solar light [6].

26.3.2 Graphitic Carbon–Nitride

Two-dimensional (2-D) graphitic carbon nitride (g-C_3N_4) has become interested due to its unique properties such as its metal-free structure, easy preparation, high thermal and chemical stability, low cost [146, 161, 181]. The g-C_3N_4 has the photocatalytic activity under the visible-light with the bandgap of 2.7 eV [334]. However the photocatalytic performance of pure g-C_3N_4 is low, due to the rapid recombination rate of the photo-generated electron–hole pair and low specific surface area, but a growing number of studies exist about improvement in the lifetime of charge carriers in the literature [62, 325].

In order to enhance the photocatalytic performance, heterostructures are formed by combining with another semiconductor suitable for the band structure of g-C_3N_4 [62]. Li et al. classified the g-C_3N_4 heterojunction structures based on the charge transfer routes and the characteristics of g-C_3N_4 as type-II, Z-scheme, S-scheme, p-n heterojunctions and Schottky heterojunctions [135]. Type II heterojunctions are constructed with metal oxides (TiO_2 [7, 278, 284, 301, 336], CuO [301], ZnO [18, 100, 281] SnO [34, 263], Fe_2O_3 [200, 244, 294], CeO_2 [154, 232], WO_3 [28, 255], metal sulfides (CdS [33, 73, 81, 132, 257, 340]), SnS_2 [324], MoS_2 [131, 260], $ZnIn_2S_4$ [131, 202, 250]), metal telluride (ZnTe [264]) which have a more positive valence band than g-C_3N_4. While type II heterojunctions are successful in improvement of the charge carriers separation, the redox activity would be weakened due to the migration of the electrons and holes to the lower level of CB and VB, respectively [209]. For this reason, the charge transfer model inspired from the green plants, g-C_3N_4 based Z-scheme heterojunctions systems have been developed to ensure efficient separation of the charge carriers and to advance the redox activity of the charges in the liquid phase [123]. The system, called the direct Z-scheme, has been developed to perform electron transfer via solid materials instead of the liquid medium [293]. One of the drawbacks of the Z-scheme heterojunction systems is that the conductor material also absorbs light, and the light-harvesting efficiency of both photocatalysts is reduced. In another drawback is; if the Fermi level of the solid conductor material which transfers the electron from the higher CB of one photocatalyst to the lower VB of the other photocatalyst is lower than the photocatalysts, a Schottky barrier forms causing the suppression of the electron flow. Besides, if the solid conductor during the synthesis is not precisely embedded between the photocatalysts, it only acts as a co-catalyst instead of charge transfer carrier [209, 292]. In order to eliminate these shortcomings, reduction photocatalyst (RP) and oxidation photocatalyst (OP) is used in g-C_3N_4 based S-scheme heterojunction systems. The internal electric field, band bending, and Coulombic attraction ensure the driving force for the charge transfer [292].

Various methods such as heat treatment, photo deposition, pyrolysis, ion exchange method, solvothermal and hydrothermal method, electrospinning method, deposition–precipitation method have been used in order to synthesize of g-C_3N_4 based materials with controllable morphology. The photocatalytic activities of the structures are summarized in Table 26.3 depending on the specific types of heterojunction with particular application, bandgap, and synthesis method for the composites.

Visible light responsive g-C_3N_4 material, which is an alternative to TiO_2 due to its unique properties, is being studied water splitting application for the efficient H_2 evolution. In order to improve the drawbacks mentioned above, type II, Z-scheme, and S-scheme heterojunction structures were developed to ensure high charges redox ability and efficient charge separation, especially in S-scheme heterojunctions, resulting in higher photocatalytic performance.

26.3.3 Carbon Quantum Dots (CQDs)

CQDs, which are zero-dimensional (0D) nanoparticles with sizes below 10 nm, are attractive because of their many unique and novel properties [295]. Their optical properties, fluorescence emissions, tunable bandgaps, and good chemical stability make it a great candidate for solar fuel applications [149]. Top-down synthesis approach with laser ablation, arc-discharge, and electrochemical oxidation, and bottom-up approach hydrothermal/solvothermal, microwave pyrolysis methods are known for the CQDs [13, 273]. During the synthesis process, the core structure of the CQDs can be functionalized with rich oxygen-containing functional groups such as carboxyl and hydroxyl [13]. That functional groups provide hybridization between CQDs and noble metals (NMs), which are turning up superior properties [65].

In solar fuel applications, CQDs increase the number of electron–hole pairs; thus, the enhancing charge transfer promotes photocatalytic activity. The hydrogen production mechanism has been depicted in four steps by using the carbon dots, as shown in Fig. 26.5. First, light irradiation and photon absorption occur; secondly, the electron in stimulated from the VB to the CB. Thirdly, the photo-produced electrons pass to the semiconductor surface, and finally, the resulting electrons and holes conduct the water-splitting process.

Table 26.3 The photocatalytic activities of the g-C_3N_4 based heterojunction type structures

g-C_3N_4 based heterojunction type	Catalyst	Synthesis method	Application	Products/activity (μmol·g^{-1}·h^{-1})	Optical bandgap (eV)	References
Type II	Ag_2S/K	Deposition	H_2 evolution	H_2/895	2.65	[323]
	r-TiO_2	Theoretical study	H_2S splitting	–	2.40	[278]
	SiC	Theoretical study	H_2 production	–	2.0	[290]
	$KNbO_3$ (100)	Theoretical study	Enhancing the photocatalytic performance	–	2.11	[155]
	ZnTe	Hydrothermal	CO_2 reduction	CH_3CH_2OH/ 17.1 μmol cm^{-2} h^{-1}	2.22	[264]
	Nb_2O_5	Pulse sonication	PEC water splitting	–	2.82	[103]
	MoS_2 QDs/ g-C_3N_4	Calcination under Ar/H_2	Degradation of methyl orange and phenol	–	2.52	[222]
	rGO/Fe_2O_3	Hydrothermal	H_2 production	H_2/6607	1.9	[244]
Z-scheme	$Bi_4O_5Br_2$	Water-induced self-assembled	H_2O_2 production of	H_2O_2/ 300 μmol cm^{-2} h^{-1} g^{-1}	2.39	[331]
	SWCNT	Two-step air etching	H_2 evolution	H_2/1346	–	[275]
	$NiMoO_4$	Calcination	CO_2 conversion	CH_4/635, CO/432, O_2/ 1853, HCOOH/647	2.31	[248]
	Cu_2O	Calcination	CO_2 conversion	CH_3OH/2.83	2.1	[330]
	ZnO/$ZnWO_4$	Calcination	CO_2 conversion		–	[342]

(continued)

Table 26.3 (continued)

$g-C_3N_4$ based heterojunction type	Catalyst	Synthesis method	Application	Products/activity (μmol·g^{-1}·h^{-1})	Optical bandgap (eV)	References
				CO/1.12, CH_4/6.24, CH_3OH/3.85, CH_3CH_2OH/1.98		
	$SnFe_2O_4$	Hydrothermal	CO_2 conversion	CO/7.56	–	[98]
	Nb-doped TiO_2	Calcination	CO_2 reduction	CH_4/562 CO/420 O_2/1702 HCOOH/698	~2.79	[247]
S-scheme	WO_3	Electrostatic self-assembly	H_2 production	H_2/982	WO_3/2.68	[61]
	$Zn_{0.2}Cd_{0.8}S$/diethylenetriamine	Solvothermal	H_2 production	H_2/6.69	$Zn_{0.2}Cd_{0.8}S$-DETA/2.48	[168]
	CdS	Calcination and hydrothermal	H_2 production	H_2/15.3	CdS/2.30	[207]
	$CuInS_2$	Hydrothermal	H_2 production	H_2/373	$CuInS_2$/1.20	[150]

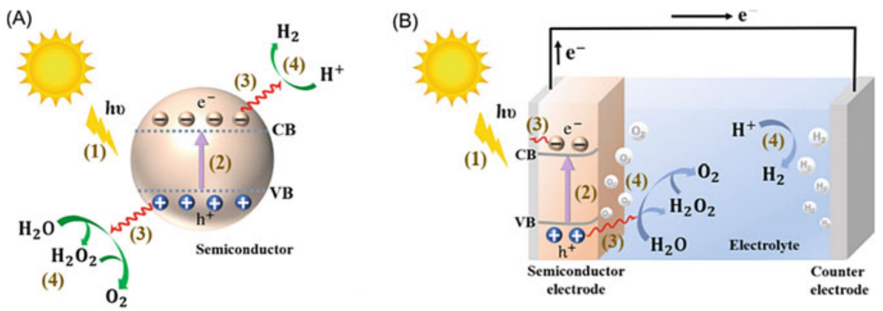

Fig. 26.5 Schematic illustration of the mechanisms for **A** photocatalytic and **B** photoelectrochemical hydrogen evolution (Reprinted from Ref. [71] with permission from Elsevier)

Sun et al. coated the Ag NPs with the CQDs to investigate the photocatalytic activity of the composite in which the highest photocatalytic obtained for AgNPs with 16% CQDs. The methanol (CH_3OH) formed as the main product by reduction of CO_2 in this reaction as 17.82 μmol after 10 h of illumination. The produced CH_3OH was three times more than the pure Ag catalyst [238]. Additionally, the dispersion effects of the CQDs prevents the NPs from the aggregation, thus increasing surface area is another crucial reason for the boosted photocatalytic activity [65]. Cobalt monoxide (CoO), which also has an aggregation problem during the synthesis, has high photocatalytic activity with 5% solar—to hydrogen efficiency (STH) [138]. Since the conversion efficiency obtained as a result of CoO/g-C_3N_4 type II heterojunction systems were not optimal [261], this system was combined with CQDs. The ternary CoO/g-C_3N_4/CQDs system showed higher photocatalytic activity with the optimum H_2 conversion rate of 987.4 μmol g^{-1} h^{-1} compare to $BiVO_4$/CQDs/CdS with 1.24 μmol/h and NiO/CQDs/$BiVO_4$ with 1.21 μmol h^{-1} [223]. The highly efficient photocatalytic activities of the carbon dots can be attributed to their electron-donating and accepting abilities, and possible active surface sites [124].

Some limiting factors to use of CQDs are the low absorption for long-wavelength, rapid decay in the initial excited state, long-term stability problem, and the weak interfacial interaction between carbon dots [149]. It is recommended that the chemical structure of the CQDs should be investigated to enhance charge transfer properties. Moreover, the future composite structures should be formed with biomaterials and copper chalcogenide structures other than metal, oxides, bismuth-based metal compounds, and carbon materials composite structures which already exist in the literature [30].

26.4 Metal Sulfide-Based Nanomaterials

Metal sulfides are one of the class of the semiconductor structures that are widely used in photocatalytic reactions for the conversion of water into hydrogen fuel using solar energy. The outstanding features; low cost, promising photocatalytic activity, long lifetime, high absorption in the visible spectrum with great mobilities of electrons and holes are the main reasons for their popularity [182]. Until today, there are various heterogeneous and hybrid structures produced with metal sulfides with superior properties for energy conversion [80].

The most commonly used structures in PEC applications of metal sulphides are CdS, ZnS, FeS_2, MoS_2, CuS, Bi_2S_3 and Sb_2S_3. Top–down and bottom–up approaches are used to synthesize these nanostructures. While the top–down approaches consist of sputtering, electrospinning, lithography, exfoliation, and milling; the bottom–up approaches have consisted of chemical vapor deposition, atomic layer deposition, pyrolysis, thermal deposition, pulsed laser deposition, micro-emulsion, precipitation, hydrothermal and solvothermal synthesis, electrodeposition, and microwave irradiation techniques [27, 36].

Especially CdS have drawn attention with the narrower direct band gap of 2.42 eV compared to TiO_2 which has 3.2 eV bandgap. Moreover, among the other sulfide structures, CdS have favorable photocatalytic performance due to the absorption wavelength, which is shorter 516 nm. This wavelength corresponds to a broader absorption spectrum, again compared with TiO_2, which absorbs the ultraviolet light with a wavelength of less than 387 nm [36]. However, the main issue that limits the use of CdS as photocatalyst is photocorrosion, lack of active sites, the high photo-generated electron–hole recombination rate [329]. Different types of heterostructures [243], co-catalysts incorporation [148], sacrificial reagents addition [72], metallic/non-metallic catalysts coupling [308] have been utilized to overcome the limitations.

Recently, Ren et al. have synthesized CdS coupled with a 2D Cu_7S_4 co-catalyst nanosheets, which increase the active sites and electron transfer yield, for photocatalytic hydrogen generation application [206]. It will be useful to consider the most striking aspects of this study based on the fundamental mechanism. The electron–hole pair of CdS nanosheets (NSs) easily recombined under irradiation, and H_2 evolution rate is lower. Efficient separation of electron–hole pairs was achieved by the presence of large contact areas, which is also shown by PL measurements between CdS/Cu_7S_4 NSs. The H_2 production for pure CdS increased from 2.6 mmol g^{-1} h^{-1} to 27.8 mmol g^{-1} h^{-1} for CdS-2% Cu_7S_4 composite. Moreover, the apparent quantum efficiency value of the composite decreased with increasing light wavelength at 420, 450, 500, and 550 nm resulted in 14.7%, 12.3%, 9.6%, and 7.2%, respectively. Light absorption wavelength of the heterostructure has affected the H_2 evolution. As another literature study, the 10 wt % CdS/g-C_3N_4 nanocomposite structure enabled the increase in the surface area and the improvement of charge separation. The H_2 evolution rate was increased to 216.48 μmol h^{-1} g^{-1}, which is four times higher compared to pure CdS [97].

However, it was found that the photocatalytic activity obtained with 20% CdS/ g-C_3N_4 nanocomposite was lower than pure CdS. This situation is attributed to the fact that the number of electrons generated electrons from g-C_3N_4 may be decreased by the shielding effect of CdS. The H_2 production rate, experimental conditions, and bandgap values of the composites which were obtained with high efficiency by using sulphide-based nanostructures including CdS and MoS_2 are shown in Table 26.4.

Zinc sulfide, which belongs to II–VI group semiconductor, has been worked as a photocatalyst due to the remarkable features such as thermal stability, nontoxicity, and lower cost [118]. It has cubic zinc blende and hexagonal wurtzite crystalline forms with the bandgap 3.72 eV and 3.77 eV, respectively [60]. As a result of this wide-bandgap, UV light absorption for electron–hole separation occurs at $\lambda < 340$ nm wavelength. In order to use the advantages of ZnS in accordance with solar fuel applications, efforts have been made to expand the light absorption in the visible wave spectrum [118].

One of the attempts to decrease the bandgap of ZnS is the use of the proper amount of dopant. For this purpose, Pang et al. modulated the electronic band structure of ZnS using Ni dopant, which is a non-toxic metal [188]. They showed that the photocatalytic CO_2 reduction activity decreased as a result of the diminishment in sulfur vacancies with the increasing amount of Ni doping. The obtained H_2 evolution was almost nine times higher with 0.1wt% Ni dopant by using full Xe arc lamp compare to pure ZnS.

The heterostructure formed by ZnS/ZnO, which has common anion, has been synthesized for increased solar fuel production [127]. The lattice mismatch (15%) between these two structures, the proposed Z-scheme system, and different annealing time for in-situ growth of ZnO directly on the ZnS enabled this structure to result in high H_2 evolution compared to pure ZnS. These results show that the particle size, shape, crystal structure, and degree of crystallinity which changes via the thermal treatment, affect the charge separation of the nanostructures alike the using various heterostructure and dopant materials.

MoS_2, a 2D structure of transition-metal dichalcogenides (TMDCs), has been widely used for solar fuel application to enhance hydrogen evolution. Its tunable bandgap within the 1.2–1.9 eV depending on the number of the sheet layers, high surface area, and abundant active sites are the advantages that make it able to be modified to increase photocatalytic activity [280]. Methods such as mechanical and chemical exfoliation, chemical vapor deposition are used in their synthesis [111]. While producing in large quantities is a drawback of mechanical exfoliation; chemical exfoliation may result in a low yield due to the wild control of the intercalation process with liquid and lithium intercalation. Besides, the toxicity of the solvents used for intercalation and long reaction time for chemical exfoliation are the other drawbacks for production of the MoS_2 [280]. CVD is the ideal method for large scale production, and it can provide high-quality MOS_2 production by controlling morphology, crystallinity, and defects [114].

MoS_2 has been used to obtain different heterostructures with other semiconductor materials which resulted in efficient solar energy conversion by changing

Table 26.4 Typical photocatalytic H_2-production systems of metal sulfides

Catalyst	Synthesis method	Products/activity (μmol·g^{-1}·h^{-1})	AQY (%)/ Wavelength (nm)	Light source	Optical bandgap (eV)	References
CdS/TiO_2	Hydrothermal	CH_4/27.85 μmol g^{-1}	–	350 W Xe lamp	CdS/2.27 TiO_2/3.04	[267]
L-Cys/CdS/NiCoP	Self-assembly	H_2/218000	76.3/420 nm	300 W Xe lamp	2.65	[92]
CdS/Ru	Deposition/precipitation	CH_4/2.585	–	0.71 W cm^{-2}	2.17	[22]
$CdS/Nb_2O_5/SnS_2$	Ultrasonication	H_2/43198 μmol g^{-1}	0.65/425	300 W Xe lamp	1.96	[162]
CdS frame-in-cage	Solution reaction	H_2/13.6	3.2/400	300 W Xe lamp	~2.3	[322]
CdS/InP	Wet impregnation	CO/216	0.44 /425	150 W Xe lamp	CdS/2.34 InP/2.20	[50]
CdS/Bi_2MoO_6	Solvothermal	H_2/6830	5.9/420	150 W Xe lamp	2.40	[29]
ZnS/CdS/ $Cd_{0.5}Zn_{0.5}S/MoS_2$	Template-assisted ion-exchange/ electrostatic assembly	H_2/50650	13.7/420	300 W Xe lamp	2.49	[237]
CoOx/N, S-C/CdS	Reflux process	H_2/40100	57.6/420	300 W Xe lamp	3.6	[258]
$Cs_{0.33}WO_3$/CdS	Precipitation	H_2/2648	–	300 W Xe lamp	2.78	[126]
CoP QDs/CdS NRs	Ultrasound	H_2/104947	32.16/420	300 W Xe lamp	CdS/2.37	[239]
CdS/$Cd_{0.5}Zn_{0.5}S$/ ZnS-$Ni(OH)_2$	Photodeposition	H_2/86790	22.8/420	300 W xenon lamp	CdS/2.42 $Cd_{0.5}Zn_{0.5}S$/ 2.52 ZnS/3.32	[211]

interfacial charge transfer properties [37]. Cho et al. obtained a few layered MoS_2/CdS QD. It was stated that the catalytic activity of the system in the hydrogen formation reaction (HER) would increase due to the enhanced carrier concentrations [37, 119, 329]. According to the results of transient absorption spectroscopy, ultrafast charge separation and long-lasting charge-separated states in heterostructures were obtained compared to bare MoS_2. In the other study, MoS_2 had been used as a co-catalyst in the heterostructure which was produced by in situ sulfidation of $CdMoO_4$ nanooctahedrons for the production of CdS/MoS_2 nanooctahedrons [329]. The pure CdS exhibited poor HER activity, and lower photocurrent density compares to bare MoS_2. Moreover, the heterostructure of CdS/MoS_2 showed highest HER activity photocurrent density. The results revealed that the heterostructure was promoting the electron transfer across the interface with the longest lifetime of photoinduced electron–hole pairs. The optimum H_2 production rate was in 27.16 mmol h^{-1} g^{-1} under visible light.

In an outstanding study in which MoS_2 was used as a co-catalyst, the H_2 production rate was obtained as 275 mmol h^{-1} g^{-1} [119]. Co-doped MoS_2/CdS structure is obtained firstly, by producing the Co crystals via pulsed laser ablation in liquid; secondly, Co dopped into a few layers of MoS_2 by ultrasonication and lastly, integrated with CdS. The synthesize steps can be seen on Fig. 26.6. The reasons to be achieved the high H_2 evolution rate by the system are; activation of the MoS_2 basal plane with the appropriate size (3.1 nm) and concentration of dopant, enhancement of the optical and electronic properties due to the crystal size of the dopant, and the exfoliation of MoS_2. Moreover, the heterostructure has demonstrated superior stability up to 5 cycles successfully for the long-term stability test.

The H_2 production rate, experimental conditions, and bandgap values of the composites which were obtained with high efficiency by using sulphide-based nanostructures except MoS_2 and CdS are shown in Table 26.5.

A novel structure, Z-scheme WO_3/CdS/WS_2 tandem heterostructure has been synthesized first embedding the WO_3 nanocrystals into WS2 nanoplate via the in-situ sulfurization of bulk WO_3 [297]. Afterwards the monodispersed CdS nanograins anchored on the ultrathin WO_3/WS_2 nanoplate. WO_3 has higher oxidation potential in the valence band, and CdS has a higher reduction potential in the conduction band. This situation makes the direct Z-scheme heterojunction possible to form between WO_3 and CdS. Additionally, WS_2 has been used as a co-catalyst which has a direct band on 1.9 eV. Its large surface area makes it easier to couple with photo absorber across the entire surface and WS_2 is the origin of the unsaturated sulfur atoms at the edges. This system efficient spatial charge separation resulted in highly efficient H_2 evolution of 14.34 mmoL h^{-1} g^{-1} with 22.96% quantum efficiency. Figure 26.7a and b shows the H_2 evolution of the pure and heterostructures for WS_2/CdS/WO_3. The pure WO_3 does not have hydrogen production because of the unsuitable conduction band potential. WO_3/WS_2 nanoplate composite, also, does not generate the H_2 due to the rapid recombination of photo-generated electrons and holes. The CW-3 (WS_2/CdS/WO_3) heterostructure

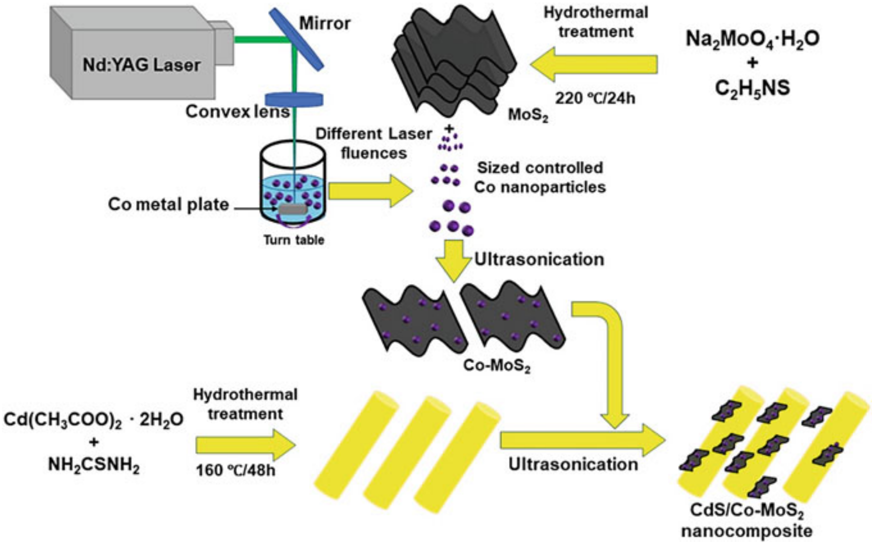

Fig. 26.6 Schematic illustration of the synthesis of CdS/Co–MoS_2 nanocomposites. Step I: Size-controlled cobalt nanocrystal synthesis via PLAL using 532-nm Nd:YAG laser with different laser fluence (0.32, 0.64, 0.96, 1.91, 2.86 and 3.82 J/cm^2). Step II: Formation of bulk MoS_2 nanosheets through hydrothermal synthesis. Step III: Formation of few-layer Co–MoS_2 nanocomposites using ultrasonication. Step IV: Integration of ultrathin Co–MoS_2 nanosheets on 1D–CdS nanorods by ultrasonication and long-time magnetic stirring to generate interfacial contact between CdS and Co–MoS_2 nanostructures (Reprinted from Ref. [119] with permission from Elsevier)

has the highest H_2 evolution rate. As well, the dosage of the 2D ultrathin WO_3/WS_2 nanoplate matrix also has a control on the photocatalytic H_2 production. As shown in Fig. 26.7c, the stability of the CW-3 composite did not decrease after six cycles, and AQE was found as 0.88% at 700 nm (Fig. 26.7d).

26.5 Transition Metal Phosphides (TMPs)

Metal transition phosphites are the superior materials that can be an alternative to noble metals with good photocatalytic performance and are even cheaper, abundant, and highly stable [279]. The photocatalytic performance increases due to the electronic structure of the phosphorus in the TMP structure [199], besides the types of different metals and the metal/phosphorus ratio also contribute to the photocatalytic activity. Other types of metal phosphites were produced for solar fuel application such as BP [246], CoP [143], Co_2P [122], Ni_2P [328], MoP [144], Cu_3P [241], FeP [53], RuP_2 [230], WP_2 [195], NbP [70] and NiCoP [92]. The electronegative nature of P atoms limits the electron delocalization of metals, which

Table 26.5 Typical photocatalytic H_2-production systems of metal sulfides

Catalyst	Synthesis method	H_2 production rate (μmol g^{-1} h^{-1})	AQY (%)/ Wavelength (nm)	Light source	Optical bandgap (eV)	References
NiS/ g-C_3N_4	Photodeposition	244	–	LED lamps	g-C_3N_4/ 2.7	[259]
ZnS/Cu	Ion-exchange	1000	17.6/ 410 ± 10	150 W Xe lamp	3.36	[44]
$Zn_{1-x}Cu_xS$	Hydrothermal	1296	2.48/365	Xe arc lamp	~3.5	[153]
WS_2/CdS/ WO_3	Hydrothermal	14,340	22.96/435	300 W Xe lamp	2.32	[297]
SnS_2/ CdS/ Nb_2O_5	Ultrasonication	55,887 μmol g^{-1}	0.65/425	300 W Xe lamp	~1.96	[162]
$CuSbS_2$	Hot-injection	2140	–		1.46	[214]
$FeCoS_2$/ CoS_2	Solvothermal	28.1 μmol h^{-1} (per o.5 mg catalyst)	–	300 W Xe lamp	–	[272]

decreases conductivity. As the P content increases, the structure can be a semi-conductor or even insulator. Electronegative P atoms trap protons and stabilize the activation of H_2 atoms attached to the surface [208]. Thus, it is known that the obtained hydrogen evolution activity is greater in CoP than Co_2P and MoP than Mo_3P [23, 286].

TMPs have relatively high photocatalytic conversion rate results in the literature studies. A heterostructure, CoxP/CdS, which has the H_2 evolution of 500 mmol g^{-1} h^{-1} was formed by the photochemical method for illumination time up to 50 min [52]. It has been observed that the conversion activity increased by 85 times compared to pure CdS with increasing illumination time. After the 50th minute, the surplus amount of Co_XP caused lowering in oxidation reaction sites on the CdS surface, resulting in lower hydrogen evolution. This indicates that composition optimization has a crucial role in modifying photocatalytic activity.

The synthesis methods of TMP nanostructures can be classified according to organic and inorganic phosphorus sources [25, 52]. The organophosphorus, tri-n-octylphosphine (TOP), and triphenylphosphine (TPP), have been used as phosphorus sources by breaking the C–P bond with high-boiling organic solvents at temperatures up to 300 °C. Thus, replacement with a metal precursor can be achieved for TMP synthesis [25]. Hypophosphites are used as inorganic P sources which are decomposed above 250 °C and following by the reaction between metal precursor and PH3 via CVD method. Alternative methods such as hydrothermal synthesis, a gas–solid response, phosphorization take place under high tempera-tures. Considering the scope of green synthesis, microwave-assisted and PH3

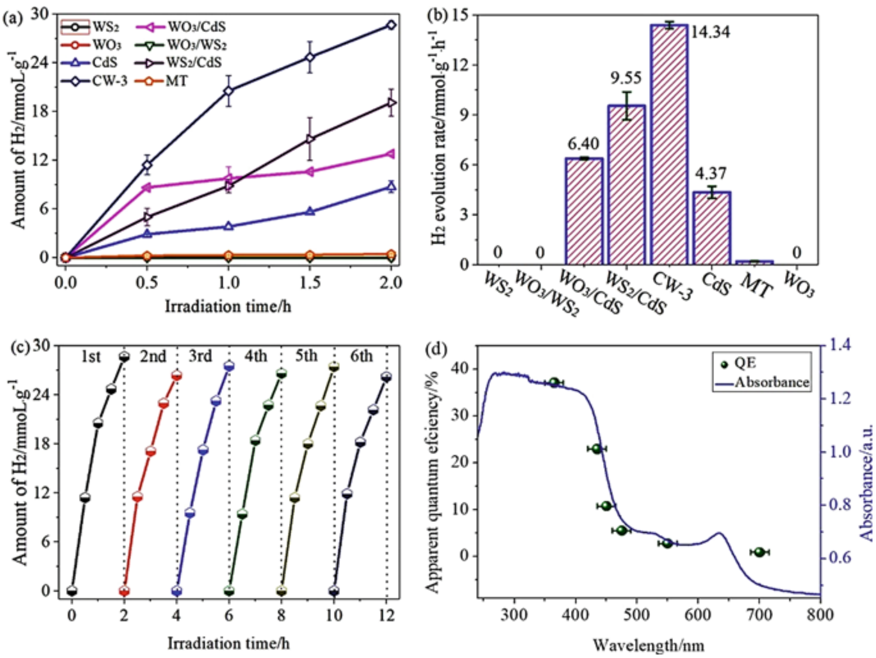

Fig. 26.7 **a** Time-dependent amounts and **b** the rates of H_2 evolution over different samples under visible light irradiation ($\lambda > 420$ nm); **c** Recycling H_2 evolution and **d** wavelength-dependent AQE of H_2 evolution from the CW-3 composite (Reprinted from Ref. [297] with permission from Elsevier)

plasma methods seem more suitable to conduct the synthesis for shorter reaction times by avoiding the high-temperature conditions [25].

The MoP is another TMP structure that draws attention with its similar electronic structure of Pt and its high conductivity [311]. In a study, it was used as a cocatalyst with CdS to construct a heterostructure [302]. The first drawback of the synthesis is the agglomeration which results due to the high-temperature phosphorization process. The second drawback originates from the TOP route due to its the toxicity, low yield, and complex operation [271]. These problems were solved by synthesizing freestanding ultra-small MoP quantum dots at low temperatures. The pyrolysis of ammonium molybdate and subsequent calcination steps at different temperatures were used for the synthesis of MoP, and then it has been dispersed with commercial CdS. The photocatalytic H_2 evolution rate of 0.60 mmol h^{-1} g^{-1} and 13.88 mmol h^{-1} g^{-1} were obtained for the pure CdS and MoP/CdS, respectively. This highly stable photocatalytic performance obtained is 1.44 times higher than Pt cocatalyst with AQY (420 nm) 66.7%.

Table 26.6 shows the synthesis methods of different TMP composite structures with high-performance hydrogen evolution rates, the conditions in which the experiments performed based on the recent literature studies.

Table 26.6 Typical photocatalytic H_2-production systems of transition metal phosphides

Catalyst	Synthesis method	H_2 production rate (μmol g^{-1} h^{-1})	AQY (%)/Wavelength (nm)	Light source	Optical bandgap (eV)	Phosphorus source	References
Cu_3P-Ni_2P/ g-C_3N_4	Hydrothermal	6526.7	18.5/400	300 W Xe lamp	1.66	Red P	[241]
MoP/g-C_3N_4	Self-assembly	327.5	10.2/420	300 W Xe lamp	–	$(NH_4)_2HPO_4$	[144]
BP/g-C_3N_4	Calcination	31.5	0.03/400	300 W Xe lamp	1.51/MoP 2.74/ g-C3N4	Red P	[246]
$Fe_xCo_{1-x}P$/CdS	Stirring	18,270	50.6/420	Visible light	1.59/ $Fe_{0.4}Co_{0.6}P$	$NaH_2PO_2 \cdot H_2O$	[318]
NixP/CuS/CdS	Photochemical deposition	18,160	0.38/420	300 W Xe lamp	–	NaH_2PO_2	[136]
InP/CdS	Wet impregnation	216	0.44 /425	150 W Xe lamp	2.34/CdS 2.20/InP	Tris(diethylamino) phosphine	[50]
$Ni_{12}P_5$/S/ $Cd_{0.5}Zn_{0.5}S$	Evaporation/deposition/ precipitation	525.5	15/420	300 W Xe lamp	2.31/ $Cd_{0.5}Zn_{0.5}S$ 2.67/S	Red P	[71]
FeP/CdS	Solvothermal	37,920	31.50/420	300 W Xe lamp	2.32/CdS	Red P	[53]
Ni_2P/MoP/ g-C_3N_4	Photodeposition	517	5.9/420	300 W Xe lamp	2.75/ g-C_3N_4	$NaH_2PO_2 \cdot H_2O$	[328]
CoP/TiO_2	Hydrothermal	604	–	300 W Xe lamp	3.11/TiO_2	$NaH_2PO_2 \cdot H_2O$	[143]
CoP QDs/CdS NRs	Ultrasound	104,947	32.16/420	300 W Xe lamp	2.37/CdS	$NaH_2PO_2 \cdot H_2O$	[239]
Co_2P/RB	Hydrothermal	5997.5	–	300 W Xe lamp	1.78/RP	Red P	[122]

26.6 Metal Oxide Frameworks (MOFs)

MOFs are the crystalline hybrid materials consisting of metal ions as inorganic metal centers connected by organic ligands [86]. Metal-organic frameworks (MOFs) materials have attracted photocatalytic H_2 generation application due to high surface area, high porosity, superior visible light absorbance, tunable bandgap, designable structure, good thermal and chemical stability [338]. However, the low conductivity of the MOFs limits their photocatalytic efficiency. The coordinatively unsaturated metal sites and the active groups on the organic linkers in MOF structures provide catalytic activity. The limits of the catalytic activity can be changed by functionalizing the metal sites, organic linkers and confining the pores [99, 142]. As an advantage, the high porosity of MOFs minimizes electron–hole recombination due to their short transport distance. The charge separation and photocatalytic activity will be increased by the addition of the electronegative structures to the MOFs [99].

MOF nanostructures can be synthesized by several methods, including solvothermal [59], layer by layer growth [1], electrochemical deposition [147], chemical vapor deposition [310], atomic/molecular layer deposition methods [172].

The incorporation of noble metals (Au [327], Ag [26], Pd [35], Pt [288], Rh [19], Ru), non-noble metals (Co [140], Cu [67], Fe [235], Ni [32]) has been carried out in previous studies in which the photocatalytic activity increased via the functionalization of the MOFs. The large pores of the MOFs provide an ideal host for nanoparticles (NPs) and single atoms (SAs). Taking advantage of this feature, NPs and/or SAs of Ru^{3+} incorporated NH_2-MIL-125/N-doped TiO_2/C was produced by using NH_2-functionalized MOF, which provides stabilization of metal cations [299]. The highest rate of H_2 evolution reached 100.0 μmol h^{-1} for NPs/SAs Ru^{3+} incorporated MOF. The evolution rate is higher than 58.3 μmol h^{-1} for Ru^{3+} composite structure where the only single atom is used, and it is higher than 83.9 μmol h^{-1}, which belongs to Pt/N-doped TiO_2 MOF material. The obtained performance has been attributed to the synergistic coupling between Ru nanoparticles and single atoms.

Nanoparticles (NPs) of noble metals (i.e. Ag, Au, Pt) which are active reaction sites can powerfully harness their surface plasmon resonance (SPR), accordingly, they absorb the visible light [262]. However, due to the high cost of the novel metals, non-noble-metal MOF analogues have been developed for high-performance catalytic activity. Moreover, the mixture of the different species of MOF heterostructures with carbon [128, 245], metal oxides [63], metal sulfides [245] covalent organic frameworks (COF) [84], phosphide [125] based materials have been produced for high photocatalytic performance. The recent studies are summarized in Table 26.7 based on the high photocatalytic performance of MOF systems.

MOFs have tunable porosity, metal centers, and organic ligands which provide advantages in their use. These properties render them the right candidate in catalytic applications such as CO_2 capture and H_2 evolution. In recent years, the studies

Table 26.7 Typical photocatalytic H_2-production systems of MOFs

Catalyst	Synthesis method	H_2 production rate (mmol g^{-1} h^{-1})	Light source	Optical bandgap (eV)	References
NH_2-UiO-66-MOF/ TpPa-1-COF	One-pot synthesis	23.41	300 W Xe lamp	2.02/ TpPa-1-COF 2.88/ NH_2-UiO-66	[314]
MOF-Cu(I)	Solvothermal	4.21	500 W Xe lamp	2.13	[31]
Pt/MIL-125-(SCH_3)	Solvothermal	3.8	350 W Xe lamp	2.69	[78]
MIL-125/g-C_3N_4/TiO_2	Calcination	0.606	300 W Xe lamp	3.04	[277]
UIO-67/Ru/Pt	Solvothermal	1.13	150 W Xe Lamp	–	[303]
NH_2-MIL-125 (Ti)/ benzoic acid-functionalized g-C_3N_4	Solvothermal	1.123	300 W Xe lamp	2.60/ NH_2-MIL-125	[337]

resulted in high conversion efficiencies by using the MOF structures. While it is an advantage to be produced especially with low cost, MOFs may have stability problems due to factors such as pH and temperature due to organic linkers [253]. Besides, material production on the industrial scale is still another limiting factor.

26.7 Summary

Today, it is known that among the usage of energy resources, renewable energy sources are in demand due to the environmental effects of non-renewable fossil fuels. Solar energy has a greater potential than the total energy of all renewable energy sources. It is quite reasonable to use H_2 as a solar fuel in order to realize the energy generation of fuels obtained from the sun, and photocatalysts are used to achieve this conversion. Nanomaterials have been used in different types and structures to understand its advantages and disadvantages, to provide high H_2 conversion, and to carry out the conversion both efficient and stable. In this chapter of the book, the semiconductor nanomaterials as metal oxides, metal–organic frameworks, carbon-based materials, metal sulfides, and phosphides have been summarized in view of their usage in photocatalytic conversion. The synthesis and design of the materials and their hybridized structures, doping, heterostructures with each other for the enhanced photocatalytic conversion were discussed in each section. It has been emphasized that each combination performs uniquely depending on both bandgaps and synergetic effects of combination with each other and also the contributions of morphology, crystallinity, composition ratios to this efficiency. The literature studies prove that the different designs of these structures and their stability, performance, and reproducibility can be changed. It can be said that in the near future, for the efficient use of solar fuels, nanomaterial engineering will proceed in the direction of structures that allow industrial production with different interfaces, morphology, and compositions.

References

1. Abbasi AR, Akhbari K, Morsali A (2012) Dense coating of surface mounted CuBTC metal–organic framework nanostructures on silk fibers, prepared by layer-by-layer method under ultrasound irradiation with antibacterial activity. Ultrason Sonochem 19(4):846–852
2. Acik M, Chabal YJ (2013) A review on thermal exfoliation of graphene oxide. J Mater Sci Res 2(1):101
3. Adegoke KA, Iqbal M, Louis H et al (2019) Synthesis, characterization and application of CdS/ZnO nanorod heterostructure for the photodegradation of Rhodamine B dye. Mater Sci Energy Technol 2(2):329–336
4. Al-Shomar SM (2020) Investigation the effect of doping concentration in Ruthenium-doped TiO_2 thin films for solar cells and sensors applications. Mater Res Express 7(3):12
5. Al Jitan S, Palmisano G, Garlisi C (2020) Synthesis and surface modification of TiO_2-based photocatalysts for the conversion of CO_2. Catalysts 10(2):30
6. Albero J, Mateo D, Garcia H (2019) Graphene-based materials as efficient photocatalysts for water splitting. Molecules 24(5):21
7. Alcudia-Ramos MA, Fuentez-Torres MO, Ortiz-Chi F et al (2020) Fabrication of g-C_3N_4/TiO_2 heterojunction composite for enhanced photocatalytic hydrogen production. Ceram Int 46(1):38–45
8. Aliaga J, Cifuentes N, Gonzalez G et al (2018) Enhancement photocatalytic activity of the heterojunction of two-dimensional hybrid semiconductors ZnO/V_2O_5. Catalysts 8(9):13
9. Ando F, Tanabe T, Gunji T et al (2018) Effect of the d-Band center on the oxygen reduction reaction activity of electrochemically dealloyed ordered intermetallic platinum-lead (PtPb) nanoparticles supported on TiO_2-deposited cup-stacked carbon nanotubes. ACS Appl Nano Mater 1(6):2844–2850
10. Ashkarran AA, Fakhari M, Hamidinezhad H et al (2015) TiO_2 nanoparticles immobilized on carbon nanotubes for enhanced visible-light photo-induced activity. J Mater Res Technol JMRT 4(2):126–132
11. Bai S, Zhang N, Gao C et al (2018) Defect engineering in photocatalytic materials. Nano Energy 53:296–336
12. Bakbolat B, Daulbayev C, Sultanov F et al (2020) Recent developments of TiO_2-based photocatalysis in the hydrogen evolution and photodegradation: a review. Nanomaterials 10 (9):16
13. Baker SN, Baker GA (2010) Luminescent carbon nanodots: emergent nanolights. Angew Chem Int Edn 49(38):6726–6744

14. Bang HJ, Lee H, Park YK et al (2020) Fabrication of Yb-doped TiO_2 using liquid phase plasma process and its photocatalytic degradation activity of naproxen. J Mater Sci 55 (23):9665–9675
15. Banin U, Waiskopf N, Hammarstrom L et al (2021) Nanotechnology for catalysis and solar energy conversion. Nanotechnology 32(4):28
16. Barreca D, Carraro G, Gasparotto A et al (2015) Fe_2O_3-TiO_2 Nano-heterostructure photoanodes for highly efficient solar water oxidation. Adv Mater Interfaces 2(17):11
17. Bayan EM, Lupeiko TG, Kolupaeva EV et al (2017) Fluorine-doped titanium dioxide: synthesis, structure, morphology, size and photocatalytic activity. In: Parinov IA, Chang SH, Jani MA (ed) Advanced materials: techniques, physics, mechanics and applications, vol 193. Springer-Verlag Berlin, Berlin, pp 17–24
18. Bayan S, Gogurla N, Midya A et al (2016) White light emission characteristics of two dimensional graphitic carbon nitride and ZnO nanorod hybrid heterojunctions. Carbon 108:335–342
19. Benseghir Y, Lemarchand A, Duguet M et al (2020) Co-immobilization of a Rh catalyst and a keggin polyoxometalate in the UiO-67 Zr-based metal-organic framework: in depth structural characterization and photocatalytic properties for CO_2 reduction. J Am Chem Soc 142(20):9428–9438
20. Bhuyan MSA, Uddin MN, Islam MM et al (2016) Synthesis of graphene. Int Nano Lett 6 (2):65–83
21. Bozkurt H, Diker H, Varlikli C Fabrication and characterization of a solution processed flexible thermal sensor by using chemically synthesized GO and rGO. In: 2019 innovations in intelligent systems and applications conference (ASYU), IEEE
22. Cai SC, Zhang M, Li JJ et al Anchoring single-atom Ru on CdS with enhanced CO_2 capture and charge accumulation for high selectivity of photothermocatalytic CO_2 reduction to solar fuels. Sol. RRL: 10
23. Callejas JF, Read CG, Popczun EJ et al (2015) Nanostructured Co_2P electrocatalyst for the hydrogen evolution reaction and direct comparison with morphologically equivalent CoP. Chem Mater 27(10):3769–3774
24. Caner N, Bulut A, Yurderi M et al (2017) Atomic layer deposition-SiO_2 layers protected PdCoNi nanoparticles supported on TiO_2 nanopowders: exceptionally stable nanocatalyst for the dehydrogenation of formic acid. Appl Catal B Environ 210:470–483
25. Cao S, Wang CJ, Fu WF et al (2017) Metal phosphides as co-catalysts for photocatalytic and photoelectrocatalytic water splitting. Chemsuschem 10(22):4306–4323
26. Chandra R, Nath M (2020) Facile synthesis of metal-organic framework (ZIF-11) and Ag NPs encapsulated-ZIF-11 composite as an effective heterogeneous catalyst for photodegradation of methylene blue. Appl Organomet Chem 34(11):19
27. Chandrasekaran S, Yao L, Deng LB et al (2019) Recent advances in metal sulfides: from controlled fabrication to electrocatalytic, photocatalytic and photoelectrochemical water splitting and beyond. Chem Soc Rev 48(15):4178–4280
28. Chang F, Zheng JJ, Wu FY et al (2019) Binary composites WO_3/g-C_3N_4 in porous morphology: facile construction, characterization, and reinforced visible light photocatalytic activity. Colloid Surf A-Physicochem Eng Asp 563:11–21
29. Chava RK, Son N, Kim YS et al (2020) Integration of perovskite type Bi(2)MoO (6)nanosheets onto one dimensional CdS: a type-II heterostructured photocatalytic system for efficient charge separation in the hydrogen evolution reaction. Inorg Chem Front 7 (15):2818–2832
30. Chen BB, Liu ML, Huang CZ (2020) Carbon dot-based composites for catalytic applications. Green Chem 22(13):4034–4054
31. Chen D-M, Sun C-X, Liu C-S et al (2018) Stable layered semiconductive Cu (I)–organic framework for efficient visible-light-driven Cr (VI) reduction and H_2 evolution. Inorg Chem 57(13):7975–7981

32. Chen JX, Xing Z, Han J et al (2020) Enhanced degradation of dyes by Cu-Co-Ni nanoparticles loaded on amino-modified octahedral metal-organic framework. J Alloy Compd 834:14
33. Chen L, Xu YM, Chen B (2019) In situ photochemical fabrication of CdS/g-C_3N_4 nanocomposites with high performance for hydrogen evolution under visible light. Appl Catal B Environ 256:8
34. Chen YF, Tang D, Wang ZH et al (2020) Sn-bridge type-II PCN/Sn/SnO heterojunction with enhanced photocatalytic activity. Semicond Sci Technol 35(11):15
35. Cheng HM, Long XY, Bian FX et al (2020) Efficient photocatalytic one-pot hydrogenation and N-alkylation of nitrobenzenes/benzonitriles with alcohols over Pd/MOFs: effect of the crystal morphology & "quasi-MOF" structure. J Catal 389:121–131
36. Cheng L, Xiang QJ, Liao YL et al (2018) CdS-Based photocatalysts. Energy Environ Sci 11 (6):1362–1391
37. Cho JS, Suwandaratne NS, Razek S et al (2020) Elucidating the mechanistic origins of photocatalytic hydrogen evolution mediated by MoS_2/CdS quantum-dot heterostructures. ACS Appl Mater Interfaces 12(39):43728–43740
38. Chowdhury MS, Rahman KS, Selvanathan V et al Current trends and prospects of tidal energy technology. Environ Dev Sustain 16
39. Chung YH, Han K, Lin CY et al (2020) Photocatalytic hydrogen production by photo-reforming of methanol with one-pot synthesized Pt-containing TiO_2 photocatalysts. Catal Today 356:95–100
40. Cifuentes B, Bustamante F, Cobo M (2019) Single and dual metal oxides as promising supports for carbon monoxide removal from an actual syngas: the crucial role of support on the selectivity of the Au-Cu system. Catalysts 9(10):25
41. Clarizia L, Andreozzi R, Apuzzo J et al (2020) Efficient acetaldehyde production and recovery upon selective Cu/TiO_2-photocatalytic oxidation of ethanol in aqueous solution. Chem Eng J 393:7
42. Cybula A, Priebe JB, Pohl MM et al (2014) The effect of calcination temperature on structure and photocatalytic properties of Au/Pd nanoparticles supported on TiO_2. Appl Catal B Environ 152:202–211
43. Das A, Patra M, Hazarika M et al (2019) ZnO-In(2)O(3)nanocomposite: an efficient solar photocatalyst. In: Kaurav N, Choudhary KK, Dixit RC, Mishra A (eds) Prof. Dinesh Varshney memorial national conference on physics and chemistry of materials, 2100. Amer Inst Physics, Melville
44. Daskalakis I, Vamvasakis I, Papadas IT et al (2020) Surface defect engineering of mesoporous Cu/ZnS nanocrystal-linked networks for improved visible-light photocatalytic hydrogen production. Inorg Chem Front 7(23):4687–4700
45. Diao W, He J, Wang Q et al (2020) K, Na and Cl co-doped TiO_2 nanorod arrays on carbon cloth for efficient photocatalytic degradation of formaldehyde under UV/visible LED irradiation. Catal Sci Technol
46. Didi A, Gomez-Calcerrada LM, Benhamou A et al (2018) Versatility in the catalytic and photocatalytic reactions of composites based on Zr- and Zr-Pd-doped titania nanoparticles. Ceram Int 44(14):17266–17276
47. Diker H, Bozkurt H, Varlikli C (2020) Dispersion stability of amine modified graphene oxides and their utilization in solution processed blue OLED. Chem Eng J 381:122716
48. Diker H, Varlikli C, Mizrak K et al (2011) Characterizations and photocatalytic activity comparisons of N-doped nc-TiO_2 depending on synthetic conditions and structural differences of amine sources. Energy 36(2):1243–1254
49. Ding L, Yang SR, Liang ZQ et al (2020) TiO_2 nanobelts with anatase/rutile heterophase junctions for highly efficient photocatalytic overall water splitting. J Colloid Interface Sci 567:181–189
50. Do KH, Kumar DP, Rangappa AP et al (2020) Indium phosphide quantum dots integrated with cadmium sulfide nanorods for photocatalytic carbon dioxide reduction. ChemCatChem 12(18):4550–4557

51. Dong F, Zhao WR, Wu ZB (2008) Characterization and photocatalytic activities of C, N and S co-doped TiO_2 with 1D nanostructure prepared by the nano-confinement effect. Nanotechnology 19(36):10
52. Dong Y, Kong L, Wang G et al (2017) Photochemical synthesis of CoxP as cocatalyst for boosting photocatalytic H_2 production via spatial charge separation. Appl Catal B 211:245–251
53. Dou M-Y, Han S-R, Du X-X et al (2020) Well-defined FeP/CdS heterostructure construction with the assistance of amine for the efficient H_2 evolution under visible light irradiation. Int J Hydrog Energy 45(56):32039–32049
54. Douven S, Mahy JG, Wolfs C et al (2020) Efficient N, Fe Co-Doped TiO_2 active under cost-effective visible LED light: from powders to films. Catalysts 10(5):22
55. Du MM, Qiu BC, Zhu QH et al (2019) Fluorine doped TiO_2/mesocellular foams with an efficient photocatalytic activity. Catal Today 327:340–346
56. El Rouby WMA, Antuch M, You SM et al (2019) Novel nano-architectured water splitting photoanodes based on TiO_2-nanorod mats surface sensitized by ZIF-67 coatings. Int J Hydrog Energy 44(59):30949–30964
57. Elhousseini MH, Isik T, Kap O et al (2020) Dual remediation of waste waters from methylene blue and chromium (VI) using thermally induced ZnO nanofibers. Appl Surf Sci 514:10
58. Eslami A, Amini MM, Yazdanbakhsh AR et al (2016) N, S co-doped TiO_2 nanoparticles and nanosheets in simulated solar light for photocatalytic degradation of non-steroidal anti-inflammatory drugs in water: a comparative study. J Chem Technol Biotechnol 91 (10):2693–2704
59. Esrafili L, Tehrani AA, Morsali A et al (2019) Ultrasound and solvothermal synthesis of a new urea-based metal-organic framework as a precursor for fabrication of cadmium (II) oxide nanostructures. Inorg Chim Acta 484:386–393
60. Fang XS, Zhai TY, Gautam UK et al (2011) ZnS nanostructures: from synthesis to applications. Prog Mater Sci 56(2):175–287
61. Fu JW, Xu QL, Low JX et al (2019) Ultrathin 2D/2D WO_3/g-C_3N_4 step-scheme H-2-production photocatalyst. Appl Catal B Environ 243:556–565
62. Fu JW, Yu JG, Jiang CJ et al (2018) g-C_3N_4-based heterostructured photocatalysts. Adv Energy Mater 8(3):31
63. Fu N, Ren XC (2020) Synthesis of double-shell hollow TiO_2@ZIF-8 nanoparticles with enhanced photocatalytic activities. Front Chem 8:10
64. Fu PF, Luan Y, Dai XG (2004) Preparation of activated carbon fibers supported TiO_2 photocatalyst and evaluation of its photocatalytic reactivity. J Mol Catal A Chem 221(1–2):81–88
65. Fu YK, Zeng GM, Lai C et al (2020) Hybrid architectures based on noble metals and carbon-based dots nanomaterials: a review of recent progress in synthesis and applications. Chem Eng J 399:22
66. Gao LK, Gan WT, Qiu Z et al (2017) Preparation of heterostructured WO_3/TiO_2 catalysts from wood fibers and its versatile photodegradation abilities. Sci Rep 7:13
67. Gao YJ, Zhang L, Gu YM et al (2020) Formation of a mixed-valence Cu(i)/Cu(ii) metal-organic framework with the full light spectrum and high selectivity of CO(2) photoreduction into CH4. Chem Sci 11(37):10143–10148
68. Garcia-Lopez E, Marci G, Pomilla FR et al (2018) ZrO_2 Based materials as photocatalysts for 2-propanol oxidation by using UV and solar light irradiation and tests for CO_2 reduction. Catal Today 313:100–105
69. Gogoi D, Namdeo A, Golder AK et al (2020) Ag-doped TiO_2 photocatalysts with effective charge transfer for highly efficient hydrogen production through water splitting. Int J Hydrog Energy 45(4):2729–2744
70. Gujt J, Zimmer P, Zysk F et al (2020) Water structure near the surface of Weyl semimetals as catalysts in photocatalytic proton reduction. Struct Dyn US 7(3):6

71. Guo M, Guo X, Lin H et al (2020) Novel noble-metal free S/Ni12P5/Cd0. 5Zn0. 5S composite with enhanced H_2 evolution activity under visible light. Int J Hydrog Energy
72. Guo Q, Liang F, Li XB et al (2019) Efficient and selective CO_2 reduction integrated with organic synthesis by solar energy. Chem 5(10):2605–2616
73. Guy N (2020) Directional transfer of photocarriers on CdS/g-C_3N_4 heterojunction modified with Pd as a cocatalyst for synergistically enhanced photocatalytic hydrogen production. Appl Surf Sci 522:12
74. Hafeez HY, Lakhera SK, Narayanan N et al (2019) Environmentally sustainable synthesis of a $CoFe_2O_4$-TiO_2/rGO ternary photocatalyst: a highly efficient and stable photocatalyst for high production of hydrogen (Solar Fuel). ACS Omega 4(1):880–891
75. Hajizadeh-Oghaz M (2019) Synthesis and characterization of Nb-La co-doped TiO_2 nanoparticles by sol-gel process for dye-sensitized solar cells. Ceram Int 45(6):6994–7000
76. Hamdi A, Ferraria AM, do Rego AMB et al (2013) Bi-Y doped and co-doped TiO_2 nanoparticles: characterization and photocatalytic activity under visible light irradiation. J Mol Catal A Chem 380:34-42
77. Han C, Wang YD, Lei YP et al (2015) In situ synthesis of graphitic-C_3N_4 nanosheet hybridized N-doped TiO_2 nanofibers for efficient photocatalytic H-2 production and degradation. Nano Res 8(4):1199–1209
78. Han SY, Pan DL, Chen H et al (2018) A Methylthio-Functionalized-MOF Photocatalyst with High Performance for Visible-Light-Driven H_2 Evolution. Angew Chem Int Ed 57 (31):9864–9869
79. Han WJ, Ren L, Zhang Z et al (2015) Graphene-supported flocculent-like TiO_2 nanostructures for enhanced photoelectrochemical activity and photodegradation performance. Ceram Int 41(6):7471–7477
80. Hao HM, Lang XJ (2019) Metal sulfide photocatalysis: visible-light-induced organic transformations. ChemCatChem 11(5):1378–1393
81. Hao XQ, Hu Y, Cui ZW et al (2019) Self-constructed facet junctions on hexagonal CdS single crystals with high photoactivity and photostability for water splitting. Appl Catal B Environ 244:694–703
82. Hasan M, Hadzifejzovi E, Rohan JF et al (2018) Electrochemcial synthesis of nanoporous hematite (α-Fe_2O_3) and their applications towards photocatalytic water oxidation. The Electrochemical Society, Glasgow, Scotland, Meeting Abstracts
83. Hassan SM, Ahmed AI, Mannaa MA (2019) Preparation and characterization of SnO_2 doped TiO_2 nanoparticles: effect of phase changes on the photocatalytic and catalytic activity. J Sci 4(3):400–412
84. He SJ, Rong QF, Niu HY et al (2019) Platform for molecular-material dual regulation: a direct Z-scheme MOF/COF heterojunction with enhanced visible-light photocatalytic activity. Appl Catal B Environ 247:49–56
85. Hezam A, Namratha K, Drmosh QA et al (2020) CeO_2 nanostructures enriched with oxygen vacancies for photocatalytic CO_2 reduction. ACS Appl Nano Mater 3(1):138–148
86. Hilal ME, Aboulouard A, Akbar AR et al (2020) Progress of MOF-derived functional materials toward industrialization in solar cells and metal-air batteries. Catalysts 10(8):31
87. Horzum N, Hilal ME, Isik T (2018) Enhanced bactericidal and photocatalytic activities of ZnO nanostructures by changing the cooling route. New J Chem 42(14):11831–11838
88. Horzum N, Mari M, Wagner M et al (2015) Controlled surface mineralization of metal oxides on nanofibers. RSC Adv 5(47):37340–37345
89. Horzum N, Munoz-Espi R, Glasser G et al (2012) Hierarchically structured metal oxide/silica nanofibers by colloid electrospinning. ACS Appl Mater Interfaces 4(11):6338–6345
90. Hu BB, Guo Q, Wang K et al (2019) Enhanced photocatalytic activity of porous In_2O_3 for reduction of CO_2 with H_2O. J Mater Sci Mater Electron 30(8):7950–7962
91. Hurtado L, Natividad R, Garcia H (2016) Photocatalytic activity of Cu_2O supported on multi layers graphene for CO_2 reduction by water under batch and continuous flow. Catal Commun 84:30–35

92. Iqbal S (2020) Spatial charge separation and transfer in L-cysteine capped NiCoP/CdS nano-heterojunction activated with intimate covalent bonding for high-quantum-yield photocatalytic hydrogen evolution. Appl Catal B Environ 274:10
93. Isık T, Hilal ME, Horzum N (2019) Green synthesis of zinc oxide nanostructures. In: Zinc oxide based nano materials and devices. IntechOpen
94. Ismael M, Wu Y, Wark M (2019) Photocatalytic activity of ZrO_2 composites with graphitic carbon nitride for hydrogen production under visible light. New J Chem 43(11):4455–4462
95. Jayasree P, Remya N (2020) Photocatalytic degradation of paracetamol using aluminosilicate supported TiO_2. Water Sci Technol 82(10):2114–2124
96. Jeon JP, Kweon DH, Jang BJ et al Enhancing the photocatalytic activity of TiO_2 catalysts. Adv Sustain Syst 19
97. Ji C, Du C, Steinkruger JD et al (2019) In-situ hydrothermal fabrication of CdS/g-C_3N_4 nanocomposites for enhanced photocatalytic water splitting. Mater Lett 240:128–131
98. Jia YF, Ma HX, Zhang WB et al (2020) Z-scheme $SnFe_2O_4$-graphitic carbon nitride: reusable, magnetic catalysts for enhanced photocatalytic CO_2 reduction. Chem Eng J 383:11
99. Jiao L, Wang Y, Jiang HL et al (2018) Metal-organic frameworks as platforms for catalytic applications. Adv Mater 30(37):23
100. Jin C, Li W, Chen YS et al (2020) Efficient photocatalytic degradation and adsorption of tetracycline over type-II heterojunctions consisting of ZnO nanorods and K-Doped exfoliated g-C_3N_4 nanosheets. Ind Eng Chem Res 59(7):2860–2873
101. Karachi N, Hosseini M, Parsaee Z et al (2018) Novel high performance reduced graphene oxide based nanocatalyst decorated with Rh_2O_3/Rh-NPs for CO_2 photoreduction. J Photochem Photobiol A Chem 364:344–354
102. Khan H, Jiang ZR, Berk D (2018) Molybdenum doped graphene/TiO_2 hybrid photocatalyst for UV/visible photocatalytic applications. Sol Energy 162:420–430
103. Khan I, Baig N, Qurashi A (2019) Graphitic carbon nitride impregnated niobium oxide (g-C3N4/Nb2O5) type (II) heterojunctions and its synergetic solar-driven hydrogen generation. ACS Appl Energy Mater 2(1):607–615
104. Khan MI, Sabir M, Mustafa GM et al (2020) 300 keV cobalt ions irradiations effect on the structural, morphological, optical and photovolatic properties of Zn doped TiO_2 thin films based dye sensitized solar cells. Ceram Int 46(10):16813–16819
105. Khojasteh H, Salavati-Niasari M, Abbasi A et al (2016) Synthesis, characterization and photocatalytic activity of PdO/TiO_2 and Pd/TiO_2 nanocomposites. J Mater Sci Mater Electron 27(2):1261–1269
106. Kim SG, Dhandole LK, Seo YS et al (2018) Active composite photocatalyst synthesized from inactive Rh & Sb doped TiO_2 nanorods: enhanced degradation of organic pollutants & antibacterial activity under visible light irradiation. Appl Catal A Gen 564:43–55
107. Kim TH, Go GM, Cho HB et al (2018) A novel synthetic method for N doped Tio(2) nanoparticles through plasma-assisted electrolysis and photocatalytic activity in the visible region. Front Chem 6:10
108. Kiss J, Sapi A, Toth M et al (2020) Rh-induced support transformation and Rh incorporation in titanate structures and their influence on catalytic activity. Catalysts 10(2):29
109. Kokorin AI, Sviridova TV, Konstantinova EA et al (2020) Dynamics of photogenerated charge carriers in TiO_2/MoO_3, TiO_2/WO_3 and TiO_2/V_2O_5 photocatalysts with mosaic structure. Catalysts 10(9):14
110. Kongsong P, Jantaporn W, Masae M (2020) Enhanced photocatalytic activity of Ni doped TiO(2)nanowire-nanoparticle hetero-structured films prepared by hydrothermal and sol-gel methods. Surf Interface Anal 52(8):486–492
111. Krishnan U, Kaur M, Singh K et al (2019) A synoptic review of MoS_2: synthesis to applications. Superlattices Microstruct 128:274–297
112. Ku Y, Lin CN, Hou WM (2011) Characterization of coupled NiO/TiO_2 photocatalyst for the photocatalytic reduction of Cr(VI) in aqueous solution. J Mol Catal A Chem 349(1–2):20–27

113. Kubacka A, Munoz-Batista MJ, Ferrer M et al (2018) Er-W codoping of TiO_2-anatase: structural and electronic characterization and disinfection capability under UV-vis, and near-IR excitation. Appl Catal B Environ 228:113–129
114. Kumar R, Sahoo S, Joanni E et al (2019) A review on synthesis of graphene, h-BN and MoS_2 for energy storage applications: recent progress and perspectives. Nano Res 12 (11):2655–2694
115. Kumaravel V, Rhatigan S, Mathew S et al (2020) Mo doped TiO_2: impact on oxygen vacancies, anatase phase stability and photocatalytic activity. J Phys Mater 3(2):15
116. Kus M, Hakli Ö, Zafer C et al (2008) Optical and electrochemical properties of polyether derivatives of perylenediimides adsorbed on nanocrystalline metal oxide films. Org Electron 9(5):757–766
117. Lee C, Wei XD, Kysar JW et al (2008) Measurement of the elastic properties and intrinsic strength of monolayer graphene. Science 321(5887):385–388
118. Lee GJ, Wu JJ (2017) Recent developments in ZnS photocatalysts from synthesis to photocatalytic applications—a review. Powder Technol 318:8–22
119. Lee H, Reddy DA, Kumar DP et al (2019) Ultra-small cobalt nanocrystals embedded in 2D-MoS_2 nano-sheets as efficient co-catalyst for solar-driven hydrogen production: study of evolution rate dependence on cobalt nanocrystal size. Appl Surf Sci 494:239–248
120. Lee MG, Kim DH, Sohn W et al (2016) Conformally coated $BiVO_4$ nanodots on porosity-controlled WO_3 nanorods as highly efficient type II heterojunction photoanodes for water oxidation. Nano Energy 28:250–260
121. Lewandowska-Bernat A, Desideri U (2018) Opportunities of power-to-gas technology in different energy systems architectures. Appl Energy 228:57–67
122. Li CY, Fu M, Wang Y et al (2020) In situ synthesis of Co_2P-decorated red phosphorus nanosheets for efficient photocatalytic H-2 evolution. Catal Sci Technol 10(7):2221–2230
123. Li HJ, Tu WG, Zhou Y et al (2016) Z-Scheme photocatalytic systems for promoting photocatalytic performance: recent progress and future challenges. Adv Sci 3(11):12
124. Li HT, Liu RH, Lian SY et al (2013) Near-infrared light controlled photocatalytic activity of carbon quantum dots for highly selective oxidation reaction. Nanoscale 5(8):3289–3297
125. Li K, Zhang Y, Lin YZ et al (2019) Versatile functional porous cobalt-nickel phosphide-carbon cocatalyst derived from a metal-organic framework for boosting the photocatalytic activity of graphitic carbon nitride. ACS Appl Mater Interfaces 11 (32):28918–28927
126. Li N, Fan HK, Dai YJ et al (2020) Insight into the solar utilization of a novel Z-scheme Cs0.33WO3/CdS heterostructure for UV-Vis-NIR driven photocatalytic hydrogen evolution. Appl Surf Sci 508:9
127. Li P, He T (2018) Common-cation based Z-scheme ZnS@ZnO core-shell nanostructure for efficient solar-fuel production. Appl Catal B-Environ 238:518–524
128. Li S, Ji K, Zhang M et al (2020) Boosting the photocatalytic CO_2 reduction of metal–organic frameworks by encapsulating carbon dots. Nanoscale 12(17):9533–9540
129. Li T, Ding DY (2020) Photoelectrochemical water splitting with black Ni/Si-doped TiO_2 nanostructures. Int J Hydrog Energy 45(41):20983–20992
130. Li WJ, Liang R, Zhou NY et al (2020) Carbon black-doped anatase TiO_2 nanorods for solar light-induced photocatalytic degradation of methylene blue. ACS Omega 5(17):10042–10051
131. Li WJ, Lin ZY, Yang GW (2017) A 2D self-assembled MoS_2/$ZnIn_2S_4$ heterostructure for efficient photocatalytic hydrogen evolution. Nanoscale 9(46):18290–18298
132. Li X, Edelmannova M, Huo PW et al (2020) Fabrication of highly stable CdS/g-C_3N_4 composite for enhanced photocatalytic degradation of RhB and reduction of CO_2. J Mater Sci 55(8):3299–3313
133. Li X, Qian JH, Xu JS et al (2018) Synthesis, characterization and electrical properties of TiO_2 modified with SiO_2 and antimony-doped tin oxide. J Mater Sci Mater Electron 29 (14):12100–12108

134. Li Y, Zhao HJ, Yang MJ (2017) TiO_2 nanoparticles supported on PMMA nanofibers for photocatalytic degradation of methyl orange. J Colloid Interface Sci 508:500–507
135. Li YF, Zhou MH, Cheng B et al (2020) Recent advances in g-C_3N_4-based heterojunction photocatalysts. J Mater Sci Technol 56:1–17
136. Li YH, Yi MY, Li JY et al (2019) Noble metal free CdS@CuS-NixP hybrid with modulated charge transfer for enhanced photocatalytic performance. Appl Catal B Environ 257:6
137. Li YY, Walsh AG, Li DS et al (2020) W-Doped TiO(2)for photothermocatalytic CO(2) reduction. Nanoscale 12(33):17245–17252
138. Liao LB, Zhang QH, Su ZH et al (2014) Efficient solar water-splitting using a nanocrystalline CoO photocatalyst. Nat Nanotechnol 9(1):69–73
139. Lin ZY, Du C, Yan B et al (2018) Two-dimensional amorphous NiO as a plasmonic photocatalyst for solar H-2 evolution. Nat Commun 9:11
140. Liu F, Cao J, Yang ZH et al (2021) Heterogeneous activation of peroxymonosulfate by cobalt-doped MIL-53 (Al) for efficient tetracycline degradation in water: coexistence of radical and non-radical reactions. J Colloid Interface Sci 581:195–204
141. Liu FY, Dai YM, Chen FH et al (2020) Lead bismuth oxybromide/graphene oxide: synthesis, characterization, and photocatalytic activity for removal of carbon dioxide, crystal violet dye, and 2-hydroxybenzoic acid. J Colloid Interface Sci 562:112–124
142. Liu M, Wu J, Hou H (2019) Metal–Organic Framework (MOF)-based materials as heterogeneous catalysts for C−H bond activation. Chem Eur J 25(12):2935–2948
143. Liu Q, Huang J, Tang H et al (2020) Construction 0D TiO_2 nanoparticles/2D CoP nanosheets heterojunctions for enhanced photocatalytic H_2 evolution activity. J Mater Sci Technol
144. Liu W, Shen J, Liu QQ et al (2018) Porous MoP network structure as co-catalyst for H-2 evolution over g-C_3N_4 nanosheets. Appl Surf Sci 462:822–830
145. Liu X, Yang J, Hu LQ et al {001}/{101} facets co-exposed TiO(2) microsheet arrays with Lanthanum doping for enhancing photocatalytic CO(2) reduction. J Mater Sci Mater Electron 11
146. Liu XL, Ma R, Zhuang L et al Recent developments of doped g-C_3N_4 photocatalysts for the degradation of organic pollutants. Crit Rev Environ Sci Technol 40
147. Liu Y, Xu N, Chen W et al (2018) Supercapacitor with high cycling stability through electrochemical deposition of metal–organic frameworks/polypyrrole positive electrode. Dalton Trans 47(38):13472–13478
148. Lu XX, Toe CY, Ji F et al (2020) Light-induced formation of MoOxSy clusters on CdS nanorods as cocatalyst for enhanced hydrogen evolution. ACS Appl Mater Interfaces 12 (7):8324–8332
149. Luo H, Guo Q, Szilagyi PA et al (2020) Carbon dots in solar-to-hydrogen conversion. Trends Chem 2(7):623–637
150. Luo JH, Lin ZX, Zhao Y et al (2020) The embedded $CuInS_2$ into hollow-concave carbon nitride for photocatalytic H_2O splitting into H-2 with S-scheme principle. Chin J Catal 41 (1):122–130
151. Luo KY, Li J, Hu WY et al (2020) Synthesizing CuO/CeO_2/ZnO ternary nano-photocatalyst with highly effective utilization of photo-excited carriers under sunlight. Nanomaterials 10 (10):13
152. Luo S, Nguyen-Phan TD, Vovchok D et al (2018) Enhanced, robust light-driven H-2 generation by gallium-doped titania nanoparticles. Phys Chem Chem Phys 20(3):2104–2112
153. Lv PW, Xu CS, Huang JJ et al (2020) Reversible photochromism for the enhancement of carrier separation in Zn1-xCuxS. J Alloy Compd 844:8
154. Ma R, Zhang S, Li L et al (2019) Enhanced visible-light-induced photoactivity of type-II CeO_2/g-C_3N_4 nanosheet toward organic pollutants degradation. ACS Sustain Chem Eng 7 (10):9699–9708
155. Ma YY, Shen YQ, Gao X et al (2019) First-principles investigation on hydrogen evolution reaction in $KNbO_3$ (100)/g-C_3N_4 heterojunction. Appl Catal A Gen 582:7

156. Macdonald TJ, Nann T (2011) Quantum dot sensitized photoelectrodes. Nanomaterials 1 (1):79–88
157. Mahy JG, Lambert SD, Tilkin RG et al (2019) Ambient temperature ZrO_2-doped TiO_2 crystalline photocatalysts: highly efficient powders and films for water depollution. Mater Today Energy 13:312–322
158. Majeed I, Nadeem MA, Badshah A et al (2017) Titania supported MOF-199 derived Cu-Cu_2O nanoparticles: highly efficient non-noble metal photocatalysts for hydrogen production from alcohol-water mixtures. Catal Sci Technol 7(3):677–686
159. Malik P, Awasthi M, Sinha S Biomass-based gaseous fuel for hybrid renewable energy systems: an overview and future research opportunities. Int J Energy Res 31
160. Malika M, Rao CV, Das RK et al (2016) Evaluation of bimetal doped TiO_2 in dye fragmentation and its comparison to mono-metal doped and bare catalysts. Appl Surf Sci 368:316–324
161. Mamba G, Mishra AK (2016) Graphitic carbon nitride (g-C_3N_4) nanocomposites: a new and exciting generation of visible light driven photocatalysts for environmental pollution remediation. Appl Catal B Environ 198:347–377
162. Mandari KK, Son N, Pandey S et al (2020) Nb_2O_5-SnS_2-CdS heteronanostructures as efficient visible-light-harvesting materials for production of H-2 under solar light irradiation. J Alloy Compd 835:15
163. Margha FH, Radwan EK, Badawy MI et al (2020) Bi2O3-$BiFeO_3$ glass-ceramic: controllable beta/gamma-Bi_2O_3 transformation and application as magnetic solar-driven photocatalyst for water decontamination. ACS Omega 5(24):14625–14634
164. Mateo D, Albero J, Garcia H (2017) Photoassisted methanation using Cu_2O nanoparticles supported on graphene as a photocatalyst. Energy Environ Sci 10(11):2392–2400
165. Mateo D, Albero J, Garcia H (2018) Graphene supported NiO/Ni nanoparticles as efficient photocatalyst for gas phase CO_2 reduction with hydrogen. Appl Catal B Environ 224:563–571
166. Mateo D, Esteve-Adell I, Albero J et al (2016) 111 oriented gold nanoplatelets on multilayer graphene as visible light photocatalyst for overall water splitting. Nat Commun 7:8
167. Mateo D, Garcia-Mulero A, Albero J et al (2019) N-doped defective graphene decorated by strontium titanate as efficient photocatalyst for overall water splitting. Appl Catal B Environ 252:111–119
168. Mei FF, Li Z, Dai K et al (2020) Step-scheme porous g-C_3N_4/Zn0.2Cd0.8S-DETA composites for efficient and stable photocatalytic H-2 production. Chin J Catal 41(1):41–49
169. Memisoglu G, Varlikli C, Diker H (2013) Solution-processed polyfluorene: naphthalenediimide–N-doped TiO_2 hybrids for ultraviolet photodetector applications. J Electron Mater 42(12):3502–3511
170. Mendiola-Alvarez SY, Guzman-Mar JL, Turnes-Palomino G et al (2019) Synthesis of Cr3+-doped TiO_2 nanoparticles: characterization and evaluation of their visible photocatalytic performance and stability. Environ Technol 40(2):144–153
171. Mendiola-Alvarez SY, Hernandez-Ramirez MA, Guzman-Mar JL et al (2019) Phosphorous-doped TiO_2 nanoparticles: synthesis, characterization, and visible photocatalytic evaluation on sulfamethazine degradation. Environ Sci Pollut Res 26(5):4180–4191
172. Meng X (2017) An overview of molecular layer deposition for organic and organic–inorganic hybrid materials: mechanisms, growth characteristics, and promising applications. J Mater Chem A 5(35):18326–18378
173. Min YX, Yang XY, Wang DW et al (2019) Tuning mixed-phase Nb-doped titania films for high-performance photocatalysts with enhanced whole-spectrum light absorption. Catal Sci Technol 9(21):6027–6036
174. Mkhalid IA, Fierro JLG, Mohamed RM et al (2020) Impact of the PtO loading on mesoporous TiO_2 nanoparticles for enhanced photodegradation of Imazapyr herbicide under simulated solar light. J Nanopart Res 22(11):14
175. Mohammed SA, Al Amouri L, Yousif E et al (2018) Synthesis of NiO:V_2O_5 nanocomposite and its photocatalytic efficiency for methyl orange degradation. Heliyon 4(3):12

176. Mondal I, Gonuguntla S, Pal U (2019) Photoinduced fabrication of Cu/TiO_2 core-shell heterostructures derived from Cu-MOF for solar hydrogen generation: the size of the Cu nanoparticle matters. J Phys Chem C 123(43):26073–26081
177. Moniz SJA, Shevlin SA, An XQ et al (2014) Fe_2O_3-TiO_2 nanocomposites for enhanced charge separation and photocatalytic activity. Chem Eur J 20(47):15571–15579
178. Muller A, Kondofersky I, Folger A et al (2017) Dual absorber Fe_2O_3/WO_3 host-guest architectures for improved charge generation and transfer in photoelectrochemical applications. Mater Res Express 4(1):9
179. Nair SB, John KA, Joseph JA et al (2020) Role of magnesium doping for ultrafast room temperature crystallization and improved photocatalytic behavior of TiO_2 nanotubes. Mater Today Proc 25:203–207
180. Naraginti S, Stephen FB, Radhakrishnan A et al (2015) Zirconium and silver co-doped TiO_2 nanoparticles as visible light catalyst for reduction of 4-nitrophenol, degradation of methyl orange and methylene blue. Spectroc Acta Pt A Molec Biomolec Spectr 135:814–819
181. Naseri A, Samadi M, Pourjavadi A et al (2017) Graphitic carbon nitride (g-C_3N_4)-based photocatalysts for solar hydrogen generation: recent advances and future development directions. J Mater Chem A 5(45):23406–23433
182. Nasir JA, Rehman ZU, Shah SNA et al (2020) Recent developments and perspectives in CdS-based photocatalysts for water splitting. J Mater Chem A 8(40):20752–20780
183. Nematollahi R, Ghotbi C, Khorasheh F et al (2020) Ni-Bi co-doped TiO_2 as highly visible light response nano-photocatalyst for CO_2 photo-reduction in a batch photo-reactor. J CO_2 Util 41:101289
184. Nguyen CC, Dinh CT, Do TO (2017) Hollow Sr/Rh-codoped TiO_2 photocatalyst for efficient sunlight-driven organic compound degradation. RSC Adv 7(6):3480–3487
185. Nguyen VH, Do HH, Nguyen TV et al (2020) Perovskite oxide-based photocatalysts for solar-driven hydrogen production: progress and perspectives. Sol Energy 211:584–599
186. Osuntokun J, Onwudiwe DC, Ebenso EE (2017) Biosynthesis and photocatalytic properties of SnO_2 nanoparticles prepared using aqueous extract of cauliflower. J Clust Sci 28(4):1883–1896
187. Panayotov DA, Yates JT (2007) Spectroscopic detection of hydrogen atom spillover from au nanoparticles supported on TiO_2: use of conduction band electrons. J Phys Chem C 111 (7):2959–2964
188. Pang H, Meng XG, Song H et al (2019) Probing the role of nickel dopant in aqueous colloidal ZnS nanocrystals for efficient solar-driven CO_2 reduction. Appl Catal B Environ 244:1013–1020
189. Pant B, Ojha GP, Kuk YS et al (2020) Synthesis and characterization of ZnO-TiO_2/carbon fiber composite with enhanced photocatalytic properties. Nanomaterials 10(10):11
190. Parrino F, Bellardita M, Garcia-Lopez EI et al (2018) Heterogeneous photocatalysis for selective formation of high-value-added molecules: some chemical and engineering aspects. ACS Catal 8(12):11191–11225
191. Paulauskas IE, Modeshia DR, Ali TT et al (2013) Photocatalytic activity of doped and undoped titanium dioxide nanoparticles synthesised by flame spray pyrolysis platinum-doped TiO_2 composites show improved activity compared to commercially available product. Platin Met Rev 57(1):32–43
192. Peng C, Wei P, Li XY et al (2018) High efficiency photocatalytic hydrogen production over ternary Cu/TiO_2@Ti_3C_2Tx enabled by low-work-function 2D titanium carbide. Nano Energy 53:97–107
193. Perez R, Perez M (2009) A fundamental look at energy reserves for the planet. The IEA SHC solar update 50(2)
194. Pham TD, Lee BK (2017) Novel photocatalytic activity of Cu@V co-doped TiO_2/PU for CO_2 reduction with H_2O vapor to produce solar fuels under visible light. J Catal 345:87–95
195. Pi MY, Wu TL, Zhang DK et al (2016) Facile preparation of semimetallic WP2 as a novel photocatalyst with high photoactivity. RSC Adv 6(19):15724–15730

196. Pierpaoli M, Zheng X, Bondarenko V et al (2019) Paving the way for a sustainable and efficient SiO_2/TiO_2 photocatalytic composite. Environments 6(8):12
197. Pillai VV, Lonkar SP, Alhassan SM (2020) Template-free, solid-state synthesis of hierarchically macroporous S-Doped TiO_2 nano-photocatalysts for efficient water remediation. ACS Omega 5(14):7969–7978
198. Pooseekheaw P, Thongpan W, Panthawan A et al (2020) Porous V_2O_5/TiO(2) nanoheterostructure films with enhanced visible-light photocatalytic performance prepared by the sparking method. Molecules 25(15):11
199. Pu Z, Liu T, Amiinu IS et al (2020) Transition-metal phosphides: activity origin, energy-related electrocatalysis applications, and synthetic strategies. Adv Funct Mater 2004009
200. Qi YH, Xu JX, Fu YL et al (2019) Metal-organic framework templated synthesis ofg-C_3N_4/Fe_2O_3@FeP composites for enhanced hydrogen production. ChemCatChem 11(15):3465–3473
201. Qian JC, Chen ZG, Chen F et al (2018) Exploration of CeO_2-CuO quantum dots in situ grown on graphene under hypha assistance for highly efficient solar-driven hydrogen production. Inorg Chem 57(23):14532–14541
202. Qin YY, Li H, Lu J et al (2020) Synergy between van der waals heterojunction and vacancy in $ZnIn_2S_4$/g-C_3N_4 2D/2D photocatalysts for enhanced photocatalytic hydrogen evolution. Appl Catal B Environ 277:10
203. Raizada P, Sudhaik A, Patial S et al (2020) Engineering nanostructures of CuO-based photocatalysts for water treatment: current progress and future challenges. Arab J Chem 13 (11):8424–8457
204. Rambabu Y, Kumar U, Singhal N et al (2019) Photocatalytic reduction of carbon dioxide using graphene oxide wrapped TiO_2 nanotubes. Appl Surf Sci 485:48–55
205. Razmyar S, Sheng T, Akter M et al (2019) Low-temperature photocatalytic hydrogen addition to two-dimensional MoO_3 nanoflakes from isopropyl alcohol for enhancing solar energy harvesting and conversion. ACS Appl Nano Mater 2(7):4180–4192
206. Ren DD, Shen RC, Jiang ZM et al (2020) Highly efficient visible-light photocatalytic H-2 evolution over 2D–2D CdS/Cu_7S_4 layered heterojunctions. Chin J Catal 41(1):31–40
207. Ren DD, Zhang WN, Ding YN et al (2020) In situ fabrication of robust cocatalyst-free CdS/g-C_3N_4 2D–2D step-scheme heterojunctions for highly active H-2 evolution. Sol RRL 4 (8):11
208. Ren XH, Philo D, Li YX et al (2020) Recent advances of low-dimensional phosphorus-based nanomaterials for solar-driven photocatalytic reactions. Coord Chem Rev 424:34
209. Rhimi B, Wang CY, Bahnemann DW (2020) Latest progress in g-C(3)N(4) based heterojunctions for hydrogen production via photocatalytic water splitting: a mini review. J Phys Energy 2(4):16
210. Rodriguez JA, Evans J, Graciani J et al (2009) High water-gas shift activity in TiO_2(110) supported Cu and Au nanoparticles: role of the oxide and metal particle size. J Phys Chem C 113(17):7364–7370
211. Ruan QQ, Ma XW, Li YY et al (2020) One-dimensional CdS@Cd0.5Zn0.5S@ZnS-Ni(OH)(2) nano-hybrids with epitaxial heterointerfaces and spatially separated photo-redox sites enabling highly-efficient visible-light-driven H(2) evolution. Nanoscale 12(39):20522–20535
212. Rusinque B, Escobedo S, de Lasa H (2020) Photoreduction of a Pd-doped mesoporous TiO_2 photocatalyst for hydrogen production under visible light. Catalysts 10(1):24
213. Sahin C, Dittrich T, Varlikli C et al (2010) Role of side groups in pyridine and bipyridine ruthenium dye complexes for modulated surface photovoltage in nanoporous TiO_2. Sol Energy Mater Sol Cells 94(4):686–690
214. Sarilmaz A, Genc E, Aslan E et al (2020) Photocatalytic hydrogen evolution via solar-driven Water splitting by $CuSbS_2$ with different shapes. J Photochem Photobiol A Chem 400:6

215. Saroj S, Singh L, Singh SV (2020) Solution-combustion synthesis of anion (iodine) doped TiO_2 nanoparticles for photocatalytic degradation of Direct Blue 199 dye and regeneration of used photocatalyst. J Photochem Photobiol A Chem 396:13
216. Schiper DE, Zhao ZH, Leitner AP et al (2017) A TiO_2/FeMnP Core/Shell nanorod array photoanode for efficient photoelectrochemical oxygen evolution. ACS Nano 11(4):4051–4059
217. Shabdan Y, Markhabayeva A, Bakranov N et al (2020) Photoactive Tungsten-Oxide Nanomaterials for Water-Splitting. Nanomaterials 10(9):37
218. Shahan M, Ahmed AM, Shehata N et al (2019) Ni-doped and Ni/Cr co-doped TiO_2 nanotubes for enhancement of photocatalytic degradation of methylene blue. J Colloid Interface Sci 555:31–41
219. Shakir I, Choi JH, Shahid M et al (2012) MoO_3-MWCNT nanocomposite photocatalyst with control of light-harvesting under visible light and natural sunlight irradiation. J Mater Chem 22(38):20549–20553
220. Shehzad N, Tahir M, Johari K et al (2018) Improved interfacial bonding of graphene-TiO_2 with enhanced photocatalytic reduction of CO_2 into solar fuel. J Environ Chem Eng 6 (6):6947–6957
221. Shi L, Benetti D, Li FY et al (2020) Phase-junction design of MOF-derived TiO_2 photoanodes sensitized with quantum dots for efficient hydrogen generation. Appl Catal B Environ 263:10
222. Shi L, He Z, Liu SQ (2018) MoS_2 quantum dots embedded in g-C_3N_4 frameworks: a hybrid 0D–2D heterojunction as an efficient visible-light driven photocatalyst. Appl Surf Sci 457:30–40
223. Shi WL, Wang JB, Yang S et al (2020) Fabrication of a ternary carbon dots/CoO/g-C_3N_4 nanocomposite photocatalyst with enhanced visible-light-driven photocatalytic hydrogen production. J Chem Technol Biotechnol 95(8):2129–2138
224. Shin HU, Lolla D, Nikolov Z et al (2016) Pd-Au nanoparticles supported by TiO_2 fibers for catalytic NO decomposition by CO. J Ind Eng Chem 33:91–98
225. Singh J, Kaur H, Kukkar D et al (2019) Green synthesis of SnO_2 NPs for solar light induced photocatalytic applications. Mater Res Express 6(11):8
226. Singh K, Harish S, Kristy AP et al (2018) Erbium doped TiO_2 interconnected mesoporous spheres as an efficient visible light catalyst for photocatalytic applications. Appl Surf Sci 449:755–763
227. Smith WA, Sharp ID, Strandwitz NC et al (2015) Interfacial band-edge energetics for solar fuels production. Energy Environ Sci 8(10):2851–2862
228. Sohail M, Baig N, Sher M et al (2020) A novel tin-doped titanium oxide nanocomposite for efficient photo-anodic water splitting. ACS Omega 5(12):6405–6413
229. Song GX, Chu ZY, Jin WQ et al (2015) Enhanced performance of g-C_3N_4/TiO_2 photocatalysts for degradation of organic pollutants under visible light. Chin J Chem Eng 23(8):1326–1334
230. Song LM, Zhang SJ (2018) RuP2/CdS photocatalysts for enhanced hydrogen evolution in water spitting and mechanism of enhancement. Powder Technol 339:479–486
231. Sorcar S, Thompson J, Hwang Y et al (2018) High-rate solar-light photoconversion of CO_2 to fuel: controllable transformation from C-1 to C-2 products. Energy Environ Sci 11 (11):3183–3193
232. Sreekanth TVM, Nagajyothi PC, Dillip GR et al (2017) Determination of band alignment in the synergistic catalyst of electronic structure-modified graphitic carbon nitride-integrated ceria quantum-dot heterojunctions for rapid degradation of organic pollutants. J Phys Chem C 121(45):25229–25242
233. Stolarczyk JK, Bhattacharyya S, Polavarapu L et al (2018) Challenges and prospects in solar water splitting and CO_2 reduction with inorganic and hybrid nanostructures. ACS Catal 8 (4):3602–3635
234. Su N, Hu XL, Zhang JB et al (2017) Plasma-induced synthesis of Pt nanoparticles supported on TiO_2 nanotubes for enhanced methanol electro-oxidation. Appl Surf Sci 399:403–410

235. Su SY, Xing ZP, Zhang SY et al (2021) Ultrathin mesoporous g-C_3N_4/NH_2-MIL-101(Fe) octahedron heterojunctions as efficient photo-Fenton-like system for enhanced photo-thermal effect and promoted visible-light-driven photocatalytic performance. Appl Surf Sci 537:11
236. Sudrajat H, Babel S, Ta AT et al (2020) Mn-doped TiO_2 photocatalysts: Role, chemical identity, and local structure of dopant. J Phys Chem Solids 144:9
237. Sun BW, Wang H, Wu JK et al (2020) Designed synthesis of unique ZnS@CdS@Cd0.5Zn0.5S-MoS_2 hollow nanospheres for efficient visible-light-driven H-2 evolution. Crystengcomm 22(16):2743–2755
238. Sun FC, Maimaiti H, Liu YE et al (2018) Preparation and photocatalytic CO_2 reduction performance of silver nanoparticles coated with coal-based carbon dots. Int J Energy Res 42 (14):4458–4469
239. Sun QQ, Yu ZB, Jiang RH et al (2020) CoP QD anchored carbon skeleton modified CdS nanorods as a co-catalyst for photocatalytic hydrogen production. Nanoscale 12(37):19203–19212
240. Sun T, Fan J, Liu EZ et al (2012) Fe and Ni co-doped TiO_2 nanoparticles prepared by alcohol-thermal method: application in hydrogen evolution by water splitting under visible light irradiation. Powder Technol 228:210–218
241. Sun WJ, Fu ZY, Shi HX et al (2020) Cu(3)P and Ni(2)P co-modified g-C(3)N(4) nanosheet with excellent photocatalytic H(2) evolution activities. J Chem Technol Biotechnol 95 (12):3117–3125
242. Suppuraja P, Parthiban S, Swaminathan M et al (2019) Hydrothermal fabrication of ternary NrGO-TiO_2/$ZnFe_2O_4$ nanocomposites for effective photocatalytic and fuel cell applications. Mater Today Proc 15:429–437
243. Teixeira IF, Quiroz J, Homsi MS et al (2020) An overview of the photocatalytic H-2 evolution by semiconductor-based materials for nonspecialists. J Braz Chem Soc 31(2):211–229
244. Thangavel N, Bellamkonda S, Arulraj AD et al (2018) Visible light induced efficient hydrogen production through semiconductor-conductor-semiconductor (S-C-S) interfaces formed between g-C_3N_4 and rGO/Fe_2O_3 core-shell composites. Catal Sci Technol 8 (19):5081–5090
245. Thi QV, Tamboli MS, Ta QTH et al (2020) A nanostructured MOF/reduced graphene oxide hybrid for enhanced photocatalytic efficiency under solar light. Mater Sci Eng B 261:114678
246. Tian B, Wu YQ, Lu GX (2021) Metal-free plasmonic boron phosphide/graphitic carbon nitride with core-shell structure photocatalysts for overall water splitting. Appl Catal B Environ 280:9
247. Truc NTT, Bach LG, Hanh NT et al (2019) The superior photocatalytic activity of Nb doped TiO_2/g-C_3N_4 direct Z-scheme system for efficient conversion of CO_2 into valuable fuels. J Colloid Interface Sci 540:1–8
248. Truc NTT, Pham TD, Nguyen MV et al (2020) Advanced $NiMoO_4$/g-C_3N_4 Z-scheme heterojunction photocatalyst for efficient conversion of CO_2 to valuable products. J Alloy Compd 842:8
249. Tseng IH, Sung YM, Chang PY et al (2017) Photocatalytic performance of titania nanosheets templated by graphene oxide. J Photochem Photobiol A Chem 339:1–11
250. Uddin A, Muhmood T, Guo ZC et al (2020) Hydrothermal synthesis of 3D/2D heterojunctions of $ZnIn_2S_4$/oxygen doped g-C_3N_4 nanosheet for visible light driven photocatalysis of 2,4-dichlorophenoxyacetic acid degradation. J Alloy Compd 845:11
251. Uma K, Muniranthinam E, Chong SH et al (2020) Fabrication of hybrid catalyst ZnO nanorod/alpha-Fe_2O_3 composites for hydrogen evolution reaction. Curr Comput Aided Drug Des 10(5):12
252. Van CN, Hai NT, Olejnicek J et al (2018) Preparation and photoelectrochemical performance of porous TiO_2/graphene nanocomposite films. Mater Lett 213:109–113
253. Verma P, Stewart DJ, Raja R (2020) Recent advances in photocatalytic CO_2 utilisation over multifunctional metal–organic frameworks. Catalysts 10(10):1176

254. Walter MG, Warren EL, McKone JR et al (2010) Solar water splitting cells. Chem Rev 110 (11):6446–6473
255. Wang CH, Qin DD, Shan DL et al (2017) Assembly of g-C_3N_4-based type II and Z-scheme heterojunction anodes with improved charge separation for photoelectrojunction water oxidation. Phys Chem Chem Phys 19(6):4507–4515
256. Wang CH, Shao CL, Zhang XT et al (2009) SnO_2 nanostructures-TiO_2 nanofibers heterostructures: controlled fabrication and high photocatalytic properties. Inorg Chem 48 (15):7261–7268
257. Wang GZ, Zhou F, Yuan BF et al (2019) Strain-tunable visible-light-responsive photocatalytic properties of two-dimensional CdS/g-C_3N_4: a hybrid density functional study. Nanomaterials 9(2):10
258. Wang JM, Xu QC, Liu ML et al (2020) The synergetic effect of N, S-codoped carbon and CoOx nanodots derived from ZIF-67 as a highly efficient cocatalyst over CdS nanorods. Sustain Energ Fuels 4(4):1954–1962
259. Wang M, Cheng JJ, Wang XF et al (2021) Sulfur-mediated photodeposition synthesis of NiS cocatalyst for boosting H-2-evolution performance of g-C_3N_4 photocatalyst. Chin J Catal 42 (1):37–45
260. Wang M, Ju P, Li JJ et al (2017) Facile synthesis of MoS_2/g-C_3N_4/GO ternary heterojunction with enhanced photocatalytic activity for water splitting. ACS Sustain Chem Eng 5(9):7878–7886
261. Wang N, Li XJ (2018) Facile synthesis of CoO nanorod/C_3N_4 heterostructure photocatalyst for an enhanced pure water splitting activity. Inorg Chem Commun 92:14–17
262. Wang P, Huang BB, Dai Y et al (2012) Plasmonic photocatalysts: harvesting visible light with noble metal nanoparticles. Phys Chem Chem Phys 14(28):9813–9825
263. Wang Q, Chen X, Tian J et al The preparation of S-SnO_2/g-C(3)N(4)heterojunction and its photocatalytic degradation of phenol and trichlorophenol. J Mater Sci Mater Electron 12
264. Wang QL, Wang XK, Yu ZH et al (2019) Artificial photosynthesis of ethanol using type-II g-C_3N_4/ZnTe heterojunction in photoelectrochemical CO_2 reduction system. Nano Energy 60:827–835
265. Wang QQ, Zhu SL, Liang YQ et al (2017) One-step synthesis of size-controlled Br-doped TiO_2 nanoparticles with enhanced visible-light photocatalytic activity. Mater Res Bull 86:248–256
266. Wang S, Wang L, Huang W (2020) Bismuth-based photocatalysts for solar energy conversion. J Mater Chem A
267. Wang SJ, Chen L, Zhao XL et al (2020) Efficient photocatalytic overall water splitting on metal-free 1D SWCNT/2D ultrathin C_3N_4 heterojunctions via novel non-resonant plasmonic effect. Appl Catal B-Environ 278:8
268. Wang XF, Li SF, Yu HG et al (2011) Ag_2O as a new visible-light photocatalyst: self-stability and high photocatalytic activity. Chem Eur J 17(28):7777–7780
269. Wang XJ, Zhao XL, Zhang DQ et al (2018) Microwave irradiation induced UIO-66-NH_2 anchored on graphene with high activity for photocatalytic reduction of CO_2. Appl Catal B-Environ 228:47–53
270. Wang XK, Wang C, Jiang WQ et al (2012) Sonochemical synthesis and characterization of Cl-doped TiO_2 and its application in the photodegradation of phthalate ester under visible light irradiation. Chem Eng J 189:288–294
271. Wang Y, Kong B, Zhao D et al (2017) Strategies for developing transition metal phosphides as heterogeneous electrocatalysts for water splitting. Nano Today 15:26–55
272. Wang Y, Wang S, Zhang SL et al (2020) Formation of hierarchical $FeCoS_2$–CoS_2 double-shelled nanotubes with enhanced performance for photocatalytic reduction of CO_2. Angew Chem
273. Wang YF, Hu AG (2014) Carbon quantum dots: synthesis, properties and applications. J Mater Chem C 2(34):6921–6939

274. Wang ZC, Song YC, Cai XF et al (2019) Rapid preparation of terbium-doped titanium dioxide nanoparticles and their enhanced photocatalytic performance. R Soc Open Sci 6 (10):14
275. Wang ZL, Chen YF, Zhang LY et al (2020) Step-scheme CdS/TiO_2 nanocomposite hollow microsphere with enhanced photocatalytic CO_2 reduction activity. J Mater Sci Technol 56:143–150
276. Wattanawikkam C, Pecharapa W (2020) Structural studies and photocatalytic properties of Mn and Zn co-doping on TiO_2 prepared by single step sonochemical method. Radiat Phys Chem 171:8
277. Wei C, Zhang W, Wang X et al (2020) MOF-derived mesoporous gC_3N_4/TiO_2 heterojunction with enhanced photocatalytic activity. Catal Lett 1–15
278. Wei SQ, Wang F, Yan P et al (2019) Interfacial coupling promoting hydrogen sulfide splitting on the staggered type II g-C_3N_4/r-TiO_2 heterojunction. J Catal 377:122–132
279. Weng C-C, Ren J-T and Yuan Z-Y (2020) Transition metal phosphide-based materials for efficient electrochemical hydrogen evolution: a critical review. ChemSusChem
280. Wu C, Zhang J, Tong X et al (2019) A critical review on enhancement of photocatalytic hydrogen production by molybdenum disulfide: from growth to interfacial activities. Small 15(35):25
281. Wu SJ, Zhao HJ, Li CF et al (2019) Type II heterojunction in hierarchically porous zinc oxide/graphitic carbon nitride microspheres promoting photocatalytic activity. J Colloid Interface Sci 538:99–107
282. Wu TS, Zhu C, Han DX et al (2019) Highly selective conversion of CO_2 to C_2H_6 on graphene modified chlorophyll Cu through multi-electron process for artificial photosynthesis. Nanoscale 11(47):22980–22988
283. Wu YA, McNulty I, Liu C et al (2019) Facet-dependent active sites of a single Cu_2O particle photocatalyst for CO_2 reduction to methanol. Nat Energy 4(11):957–968
284. Wu YX, Liu LM, An XQ et al (2019) New insights into interfacial photocharge transfer in TiO_2/C_3N_4 heterostructures: effects of facets and defects. New J Chem 43(11):4511–4517
285. Xia Y, Cheng B, Fan JJ et al (2019) Unraveling photoexcited charge transfer pathway and process of CdS/graphene nanoribbon composites toward visible-light photocatalytic hydrogen evolution. Small 15(34):9
286. Xiao Z, Bi C, Shao Y et al (2014) Efficient, high yield perovskite photovoltaic devices grown by interdiffusion of solution-processed precursor stacking layers. Energy Environ Sci 7(8):2619–2623
287. Xie W, Li R, Xu QY (2018) Enhanced photocatalytic activity of Se-doped TiO_2 under visible light irradiation. Sci Rep 8:10
288. Xing HM, Teng SY, Xing ZH et al (2020) Effect of Pt cocatalyst on visible light driven hydrogen evolution of anthracene-based zirconium metal-organic framework. Appl Surf Sci 532:7
289. Xing M, Zhang J, Qiu B et al (2015) A brown mesoporous TiO_2-x/MCF composite with an extremely high quantum yield of solar energy photocatalysis for H_2 evolution. Small 11 (16):1920–1929
290. Xu L, Li Q, Li XF et al (2019) Rationally designed 2D/2DSiC/g-C_3N_4 photocatalysts for hydrogen production. Catal Sci Technol 9(15):3896–3906
291. Xu M, Wu H, Tang YW et al (2020) One-step in-situ synthesis of porous Fe3+-doped TiO_2 octahedra toward visible-light photocatalytic conversion of CO_2 into solar fuel. Microporous Mesoporous Mat 309:7
292. Xu QL, Zhang LY, Cheng B et al (2020) S-Scheme Heterojunction Photocatalyst. Chem 6 (7):1543–1559
293. Xu QL, Zhang LY, Yu JG et al (2018) Direct Z-scheme photocatalysts: principles, synthesis, and applications. Mater Today 21(10):1042–1063
294. Xu QL, Zhu BC, Jiang CJ et al (2018) Constructing 2D/2D Fe_2O_3/g-C_3N_4 direct Z-scheme photocatalysts with enhanced H-2 generation performance. Sol RRL 2(3):10

295. Xu XY, Ray R, Gu YL et al (2004) Electrophoretic analysis and purification of fluorescent single-walled carbon nanotube fragments. J Am Chem Soc 126(40):12736–12737
296. Xu YH, Liang DH, Liu ML et al (2008) Preparation and characterization of Cu_2O-TiO_2: Efficient photocatalytic degradation of methylene blue. Mater Res Bull 43(12):3474–3482
297. Xue C, Zhang P, Shao GS et al (2020) Effective promotion of spacial charge separation in direct Z-scheme WO3/CdS/WS2 tandem heterojunction with enhanced visible-light-driven photocatalytic H-2 evolution. Chem Eng J 398:10
298. Yadav V, Verma P, Sharma H et al (2020) Photodegradation of 4-nitrophenol over B-doped TiO_2 nanostructure: effect of dopant concentration, kinetics, and mechanism. Environ Sci Pollut Res 27(10):10966–10980
299. Yan BL, Liu DP, Feng XL et al (2020) Ru species supported on MOF-derived N-doped TiO_2/C hybrids as efficient electrocatalytic/photocatalytic hydrogen evolution reaction catalysts. Adv Func Mater 30(31):9
300. Yan BL, Zhang LJ, Tang ZY et al (2017) Palladium-decorated hierarchical titania constructed from the metal-organic frameworks NH_2-MIL-125(Ti) as a robust photocatalyst for hydrogen evolution. Appl Catal B-Environ 218:743–750
301. Yan MY, Jiang ZY, Zheng JM et al (2020) Theoretical study on transport-scheme conversion of g-C_3N_4/TiO_2 heterojunctions by oxygen vacancies. Appl Surf Sci 531:7
302. Yang F, Liu D, Li Y, et al Solid-state synthesis of ultra-small freestanding amorphous MoP quantum dots for highly efficient photocatalytic H_2 production. Chem Eng J 406:126838
303. Yang S, Fan D, Hu W et al (2018) Elucidating charge separation dynamics in a hybrid metal-organic framework photocatalyst for light-driven H_2 evolution. J Phys Chem C 122 (6):3305–3311
304. Yang XH, Wang Y, Zhang LT et al (2020) The use of tunable optical absorption plasmonic Au and Ag decorated TiO_2 structures as efficient visible light photocatalysts. Catalysts 10 (1):14
305. Yang Y, Zhang C, Lai C et al (2018) BiOX (X = Cl, Br, I) photocatalytic nanomaterials: applications for fuels and environmental management. Adv Colloid Interface Sci 254:76–93
306. Yang YJ, Yu YL, Wang JS et al (2017) Doping and transformation mechanisms of Fe_3+ ions in Fe-doped TiO_2. CrystEngComm 19(7):1100–1105
307. Yi LH, Lan FJ, Li JE et al (2018) Efficient noble-metal-free Co-NG/TiO_2 photocatalyst for H-2 evolution: synergistic effect between single-atom Co and N-doped graphene for enhanced photocatalytic activity. ACS Sustain Chem Eng 6(10):12766–12775
308. Yi SS, Zhang XB, Wulan BR et al (2018) Non-noble metals applied to solar water splitting. Energy Environ Sci 11(11):3128–3156
309. Yoon JW, Kim DH, Kim JH et al (2019) NH_2-MIL-125(Ti)/TiO_2 nanorod heterojunction photoanodes for efficient photoelectrochemical water splitting. Appl Catal B-Environ 244:511–518
310. Young C, Wang J, Kim J et al (2018) Controlled chemical vapor deposition for synthesis of nanowire arrays of metal–organic frameworks and their thermal conversion to carbon/metal oxide hybrid materials. Chem Mater 30(10):3379–3386
311. Yu P, Wang F, Shifa TA et al (2019) Earth abundant materials beyond transition metal dichalcogenides: a focus on electrocatalyzing hydrogen evolution reaction. Nano Energy 58:244–276
312. Yuan J, Zhang JJ, Yang MP et al (2018) CuO nanoparticles supported on TiO_2 with high efficiency for CO_2 electrochemical reduction to ethanol. Catalysts 8(4):11
313. Zang YP, Li LP, Xu YS et al (2014) Hybridization of brookite TiO_2 with g-C_3N_4: a visible-light-driven photocatalyst for As_3+ oxidation, MO degradation and water splitting for hydrogen evolution. J Mater Chem A 2(38):15774–15780
314. Zhang FM, Sheng JL, Yang ZD et al (2018) Rational design of MOF/COF hybrid materials for photocatalytic H_2 evolution in the presence of sacrificial electron donors. Angew Chem Int Edn 57(37):12106–12110

315. Zhang GX, Song AK, Duan YW et al (2018) Enhanced photocatalytic activity of TiO_2/zeolite composite for abatement of pollutants. Microporous Mesoporous Mat 255:61–68
316. Zhang H, Tang Q, Li QS et al (2020) Enhanced photocatalytic properties of PET filaments coated with Ag-N Co-doped TiO_2 nanoparticles sensitized with disperse blue dyes. Nanomaterials 10(5):24
317. Zhang HY, Wang ZW, Li RN et al (2017) TiO_2 supported on reed straw biochar as an adsorptive and photocatalytic composite for the efficient degradation of sulfamethoxazole in aqueous matrices. Chemosphere 185:351–360
318. Zhang J, Zhao Q, Zhang JX et al (2020) Highly active FexCo1-xP cocatalysts modified CdS for photocatalytic hydrogen production. Int J Hydrog Energy 45(43):22722–22731
319. Zhang JF, Zhou P, Liu JJ et al (2014) New understanding of the difference of photocatalytic activity among anatase, rutile and brookite TiO_2. Phys Chem Chem Phys 16(38):20382–20386
320. Zhang L, Wang WZ, Sun SM et al (2013) Solar light photocatalysis using Bi_2O_3/Bi_2SiO_5 nanoheterostructures formed in mesoporous SiO_2 microspheres. CrystEngComm 15 (46):10043–10048
321. Zhang P, Lu XF, Luan D et al (2020) Fabrication of heterostructured Fe_2TiO_5–TiO_2 nanocages with enhanced photoelectrochemical performance for solar energy conversion. Angew Chem 132(21):8205–8209
322. Zhang P, Luan DY, Lou XW (2020) Fabrication of CdS frame-in-cage particles for efficient photocatalytic hydrogen generation under visible-light irradiation. Adv Mater 32(39):6
323. Zhang QL, Chen PF, Chen L et al (2020) Facile fabrication of novel Ag_2S/K-g-C_3N_4 composite and its enhanced performance in photocatalytic H-2 evolution. J Colloid Interface Sci 568:117–129
324. Zhang R, Bi LL, Wang DJ et al (2020) Investigation on various photo-generated carrier transfer processes of SnS_2/g-C_3N_4 heterojunction photocatalysts for hydrogen evolution. J Colloid Interface Sci 578:431–440
325. Zhang S, Gu PC, Ma R et al (2019) Recent developments in fabrication and structure regulation of visible-light-driven g-C_3N_4-based photocatalysts towards water purification: a critical review. Catal Today 335:65–77
326. Zhang XY, Li L, Zhou QL et al (2019) Facile synthesis of novel gully-like double-sized mesoporous structural Sr-doped ZrO_2-TiO_2 composites with improved photocatalytic efficiency. J Solid State Chem 269:375–385
327. Zhang YM, Song J, Shao WH et al (2021) Au@NH2-MIL-125(Ti) heterostructure as light-responsive oxidase-like mimic for colorimetric sensing of cysteine. Microporous Mesoporous Mat 310:9
328. Zhao J, Fu B, Li X et al (2020) Construction of the Ni_2P/MoP heterostructure as a high-performance cocatalyst for visible-light-driven hydrogen production. ACS Appl Energy Mater
329. Zhao L, Dong T, Du J et al (2020) Synthesis of CdS/MoS_2 nanooctahedrons heterostructure with a tight interface for enhanced photocatalytic H_2 evolution and biomass upgrading. Sol. RRL: 2000415
330. Zhao X, Fan YY, Zhang WS et al (2020) Nanoengineering construction of Cu_2O nanowire arrays encapsulated with g-C_3N_4 as 3D spatial reticulation all-solid-state direct Z-Scheme photocatalysts for photocatalytic reduction of carbon dioxide. ACS Catal 10(11):6367–6376
331. Zhao XS, You YY, Huang SB et al (2020) Z-scheme photocatalytic production of hydrogen peroxide over $Bi_4O_5Br_2$/g-C_3N_4 heterostructure under visible light. Appl Catal B-Environ 278:11
332. Zhao YX, Yang BF, Xu J et al (2012) Facile synthesis of Ag nanoparticles supported on TiO_2 inverse opal with enhanced visible-light photocatalytic activity. Thin Solid Films 520 (9):3515–3522
333. Zhao ZW, Zhang WD, Lv XS et al (2016) Noble metal-free Bi nanoparticles supported on TiO_2 with plasmon-enhanced visible light photocatalytic air purification. Environ Sci Nano 3 (6):1306–1317

334. Zheng Y, Liu J, Liang J et al (2012) Graphitic carbon nitride materials: controllable synthesis and applications in fuel cells and photocatalysis. Energy Environ Sci 5(5):6717–6731
335. Zhong YM, Yang SY, Cai X et al (2020) Bio-inspired multilayered graphene-directed assembly of monolithic photo-membrane for full-visible light response and efficient charge separation. Appl Catal B-Environ 263:13
336. Zhou BX, Ding SS, Wang Y et al (2020) Type-II/type-II band alignment to boost spatial charge separation: a case study of g-C_3N_4 quantum dots/a-TiO_2/r-TiO_2 for highly efficient photocatalytic hydrogen and oxygen evolution. Nanoscale 12(10):6037–6046
337. Zhou G, Wu M-F, Xing Q-J et al (2018) Synthesis and characterizations of metal-free semiconductor/MOFs with good stability and high photocatalytic activity for H_2 evolution: a novel Z-scheme heterostructured photocatalyst formed by covalent bonds. Appl Catal B 220:607–614
338. Zhou H-C, Long JR, Yaghi OM (2012) Introduction to metal–organic frameworks, ACS Publications
339. Zhou X, Cui SC, Liu JG (2020) Three-dimensional graphene oxide cross-linked by benzidine as an efficient metal-free photocatalyst for hydrogen evolution. RSC Adv 10 (25):14725–14732
340. Zhou XF, Fang YX, Cai X et al (2020) In situ photodeposited construction of Pt-CdS/g-C3N4-MnOx composite photocatalyst for efficient visible-light-driven overall water splitting. ACS Appl Mater Interfaces 12(18):20579–20588
341. Zhu LL, Hong MH, Ho GW (2015) Hierarchical assembly of SnO_2/ZnO nanostructures for enhanced photocatalytic performance. Sci Rep 5:11
342. Zhu LY, Li H, Xu QL et al (2020) High-efficient separation of photoinduced carriers on double Z-scheme heterojunction for superior photocatalytic CO_2 reduction. J Colloid Interface Sci 564:303–312
343. Zhu XD, Pei LX, Zhu RR et al (2018) Preparation and characterization of Sn/La co-doped TiO_2 nanomaterials and their phase transformation and photocatalytic activity. Sci Rep 8:14
344. Zhu YH, Yao Y, Luo Z et al (2020) Nanostructured MoO_3 for efficient energy and environmental catalysis. Molecules 25(1):26
345. Zhu ZZ, Han Y, Chen CP et al (2018) Reduced graphene oxide-cadmium sulfide nanorods decorated with silver nanoparticles for efficient photocatalytic reduction carbon dioxide under visible light. ChemCatChem 10(7):1627–1634